A stratospheric aerosol climatology from SAGE II and CLAES measurements: 1. Methodology

J. J. Bauman and P. B. Russell
NASA Ames Research Center, Moffett Field, California, USA

M. A. Geller
State University of New York, Stony Brook, New York, USA

Patrick Hamill
San Jose State University, San Jose, California, USA

Received 27 September 2002; accepted 29 January 2003; published 8 July 2003.

[1] This paper presents the methods used to produce a global climatology of the stratospheric aerosol using data from two satellite instruments: the Stratospheric Aerosol and Gas Experiment (SAGE II) and the Cryogenic Limb Array Etalon Spectrometer (CLAES). The climatology, which spans from December 1984 to August 1999, includes values and uncertainties of measured extinction and optical depth and of retrieved particle effective radius R_{eff}, distribution width σ_g, surface area S, and volume V. As a basis for aerosol retrievals, a multiwavelength look-up table (LUT) algorithm was developed that matches the satellite-measured extinction ratios to precomputed ratios that are based on a range of unimodal lognormal size distributions. For cases in which the LUT does not find an acceptable match between measured and precomputed extinction spectra, a different technique called the parameter search technique is utilized. The combination of these two techniques and data from both satellites allows us to retrieve values of R_{eff}, σ_g, S, and V over a wider range of conditions and from a wider range of wavelengths than used by other methods. This greater wavelength range helps constrain retrieved results, especially in postvolcanic conditions when particle sizes are greatly increased and SAGE II extinction spectra become essentially independent of wavelength. Our method includes an altitude- and time-dependent procedure that uses bimodal size distributions from in situ measurements to estimate bias and uncertainty introduced by assuming a unimodal functional form. Correcting for this bias reduces uncertainty in retrievals of R_{eff}, S, and V by about 7%, 5%, and 1% (averaged over all altitude bands), leaving remaining uncertainties from the unimodal assumption of about ±18%, ±20%, and ±21%, respectively. Additional uncertainties, resulting from measurement error and spatiotemporal variability, are evaluated by propagating input uncertainties through the retrieval algorithm. In an accompanying paper we report on a climatology of R_{eff}, S, and V and consider uncertainties in our retrieved values of these parameters. In this paper we examine the sensitivity of our retrievals to refractive index and measurement wavelength. We find, for example, that changing refractive index from a value for the stratospheric temperature of 215 K to that for 300 K can increase retrieved R_{eff} by ~7.5%, owing largely to effects at the CLAES 12.82 μm wavelength. When only SAGE II wavelengths are used, corresponding changes in R_{eff} are much smaller. *INDEX TERMS:* 0305 Atmospheric Composition and Structure: Aerosols and particles (0345, 4801); 0340 Atmospheric Composition and Structure: Middle atmosphere—composition and chemistry; 0370 Atmospheric Composition and Structure: Volcanic effects (8409); 0394 Atmospheric Composition and Structure: Instruments and techniques; 3309 Meteorology and Atmospheric Dynamics: Climatology (1620); *KEYWORDS:* stratospheric aerosols, volcanic aerosol and climate response, aerosol-climate interaction, effective radius, SAGE II, CLAES

Citation: Bauman, J. J., P. B. Russell, M. A. Geller, and P. Hamill, A stratospheric aerosol climatology from SAGE II and CLAES measurements: 1. Methodology, *J. Geophys. Res.*, *108*(D13), 4382, doi:10.1029/2002JD002992, 2003.

0148-0227/03/2002JD002992$09.00

1. Introduction

[2] Research over the past few decades has provided overwhelming evidence that the presence of aerosol particles in the stratosphere can significantly impact atmospheric chemistry, dynamics, radiation and climate (e.g., *Rampino and Self* [1984], *Hofmann and Solomon* [1989], *Robock* [1991], *Dutton and Christy* [1992], *Jensen and Toon* [1992], *Kinne et al.* [1992], *Lacis et al.* [1992], *Prather* [1992], *Minnis et al.* [1993], *McCormick et al.* [1995], and many others). The stratospheric aerosol can cool the Earth's troposphere and surface by scattering incoming short-wave radiation and can warm the lower stratosphere by absorbing outgoing long-wave radiation [*Hansen et al.*, 1990]. Aerosols can also affect climate by enhancing upward air motion in the lower stratosphere and altering stratospheric dynamics [*Kinne et al.*, 1992; *Young et al.*, 1994], by modifying upper tropospheric cirrus microphysical properties [*Jensen and Toon*, 1992], and by providing effective sites for heterogeneous chemical reactions that promote the depletion of ozone in the lower stratosphere [*Hofmann and Solomon*, 1989; *Brasseur et al.*, 1990]. The evidence of their climatic importance makes a compelling case for improved efforts to obtain accurate information about the global distribution and characteristics of stratospheric aerosols. A knowledge of the physical properties of the stratospheric aerosol is also important in analyzing data from space-borne instruments whose measurements are affected by the presence of the layer.

[3] In response to this need, we have used data from the Stratospheric Aerosol and Gas Experiment (SAGE II) and the Cryogenic Limb Array Etalon Spectrometer (CLAES) satellite borne instruments to develop a climatology of the stratospheric aerosol. In this paper we describe the method used to generate the climatology. We present the climatology and a comparison to previous climatologies in the companion paper, *Bauman et al.* [2003] (hereinafter referred to as paper 2). Our climatology includes values and uncertainties of measured extinction and optical depth at the four SAGE II wavelengths (0.385, 0.453, 0.525 and 1.02 μm) and, when available, at the CLAES 12.82 μm wavelength. Our study covers the 14 year, 9 month period from December 1984 to August 1999; of this period the CLAES data are available for the important 17 month period January 1992 through May 1993, when particle sizes had been greatly increased by the Pinatubo volcanic injection. We have evaluated optical depths by integrating the extinction from two kilometers above the tropopause to the highest altitude in the SAGE II record, 40.5 km. Also included are retrieved particle effective radius R_{eff}, distribution width σ_g, surface area S and volume V. As a basis for aerosol retrievals, a multiwavelength look-up table (LUT) algorithm was developed that uses a combination of 4-wavelength SAGE II extinction spectra and, when available, the CLAES 12.82 μm extinction measurements. We use the LUT to compare satellite-measured extinction ratios to precomputed extinction ratios based on Mie scattering calculations. (Note that when we refer to "extinction ratio" we mean the ratio of the extinction at one wavelength to the extinction at another wavelength.) The precomputed ratios were determined for a range of unimodal lognormal size distributions by varying the values of σ_g and R_{eff}. Specifically, σ_g was varied between 1.1 and 3.4, while R_{eff} was varied from 0.1 to 2.0 μm. Using a range of size distribution parameters enables the LUT algorithm to propagate the uncertainties in extinction measurements to corresponding uncertainties in retrieved R_{eff}, S and V.

[4] The LUT algorithm can retrieve some information about distribution width σ_g by noting the range of σ_g values for which computed extinction spectra are consistent with SAGE II and CLAES measurements. We use the statistical parameter χ^2 (defined below) as a measure of the consistency between computed and measured optical depth. Our criterion for consistency is that the values of χ^2 obtained by comparing measured extinctions with those calculated by the LUT for a given value of σ_g must be less than or equal to the number of measurement wavelengths. (See section 4 for details.) For values of σ_g that do not meet this χ^2 criterion, an alternative approach, the Parameter Search Technique (PST), is used to search for values of R_{eff} consistent with SAGE II and CLAES extinction measurements. The PST varies the three parameters, R_{eff}, σ_g and N_o, of a unimodal distribution to obtain a best fit with extinction measurements. Both the χ^2 criterion and the PST are incorporated into the LUT algorithm to retrieve information about size distribution width from extinction measurements. A complete listing of the computer program that implements the combined LUT-PST algorithm is given by *Bauman* [2000] (available at ftp://science.arc.nasa.gov/pub/aats/pub/jill_bauman/Bauman-Dissertation-Aug2000.pdf).

[5] Size distribution measurements by *Deshler et al.* [1993] and *Deshler and Oltmans* [1998] reveal that during a period of strong volcanic influence, stratospheric aerosol distributions tend to be large-mode-dominant bimodal (i.e., the large mode makes the dominant contribution to surface area S). During near-background periods, distributions range from unimodal to small-mode-dominant bimodal. Retrievals by the LUT are based on unimodal distributions. Therefore, as shown in section 7, the LUT algorithm includes an altitude- and time-dependent procedure to estimate and remove the bias introduced by assuming a unimodal functional form.

2. Look-Up Table Algorithm

[6] The look-up table (LUT) algorithm retrieves values and uncertainties of particle effective radius R_{eff}, surface area S and volume V by comparing ratios of measured extinction and optical depth spectra from SAGE II and CLAES to theoretical ratios that are precomputed for a range of unimodal lognormal size distributions. In this section we present the derivation of the theoretical, or precomputed ratios. The details of comparing the measured to the theoretical ratios are given in section 3.

[7] In our LUT approach we approximate the stratospheric aerosol size distribution as unimodal lognormal which can be expressed as:

$$\frac{dN(r)}{dr} = \frac{N_o}{r \ln \sigma_g \sqrt{2\pi}} \exp\left[-\frac{\ln^2 (r/r_g)}{2 \ln^2 \sigma_g} \right]. \qquad (1)$$

Here r is the particle radius, dN is number of particles per unit volume with radii between r and $r + dr$, N_o is the total

Table 1. Complex Refractive Index at 215 K for the SAGE II and CLAES Wavelengths[a]

λ, μm	n	K	Source
0.385	1.46767	*	*Palmer and Williams* [1975]
0.453	1.45079	*	*Palmer and Williams* [1975]
0.525	1.44957	*	*Palmer and Williams* [1975]
1.020	1.43875	*	*Palmer and Williams* [1975]
7.955	1.15958	0.4319	*Tisdale et al.* [1998]
12.82	1.76558	0.2976	*Tisdale et al.* [1998]

[a]Indices from *Palmer and Williams* [1975] include a Lorentz-Lorenz temperature correction from 300 K to 215 K and are interpolated to 70.85% H_2SO_4, assuming the environment contains 3 ppmv of water. The imaginary indices (k) marked * are $\leq 10^{-6}$. The complex indices from *Tisdale et al.* [1998] are interpolated to 70.85% H_2SO_4.

number of particles per unit volume, σ_g is the geometric standard deviation or width of the distribution, and r_g is the geometric mean radius. (Note, r_g is often referred to as the mode radius. However, the mode radius of dN/dr is $r_g \exp(-\ln^2 \sigma_g)$ [*Dennis*, 1976]). The unimodal lognormal distribution has three adjustable fitting parameters: r_g, σ_g, and N_o. Several studies indicate that nonvolcanic stratospheric aerosol size distributions are well approximated by this functional form [*Pueschel et al.*, 1989; *Yue et al.*, 1994]. However, *Deshler et al.* [1993] show that postvolcanic stratospheric size distributions are typically bimodal. The effects of assuming a unimodal lognormal size distribution on retrieval accuracy are discussed in section 7.

[8] A parameter that is frequently used to describe particle size is the effective, or area-weighted radius, R_{eff}, defined as the ratio of the third moment to the second moment of the size distribution [*Hansen and Travis*, 1974]:

$$R_{eff} = M_3/M_2. \tag{2}$$

The size distribution moment M_n, is defined as:

$$M_n = \int_0^\infty \frac{dN(r)}{dr} r^n dr. \tag{3}$$

Hansen and Travis [1974] have shown that R_{eff} is a useful parameter for describing radiative-transfer properties of a variety of aerosols. An analytical expression for the *nth* moment M_n of a unimodal lognormal distribution can be derived by combining equations (1) and (3) [*Lenoble and Brogniez*, 1984]:

$$M_n = N_o r_g^n \exp\left[\left(n^2/2\right)\left(\ln^2 \sigma_g\right)\right]. \tag{4}$$

This expression can then be used with equation (2) to redefine R_{eff} in terms of the lognormal fitting parameters:

$$R_{eff} = r_g \exp\left[2.5 \ln^2 \sigma_g\right]. \tag{5}$$

This shows that for a unimodal lognormal size distribution of fixed width σ_g, a unique relationship exists between the geometric mean radius r_g and the effective radius R_{eff}.

[9] The extinction due to aerosols is related to $dN(r)/dr$ through Mie scattering theory. If the aerosols are homogeneous spheres of size r and refractive index m_λ, the aerosol extinction coefficient $\beta(\lambda)$ at wavelength λ can be calculated as follows:

$$\beta(\lambda) = \int_0^\infty \pi r^2 Q_e(\lambda, r, m_\lambda) \frac{dN(r)}{dr} dr. \tag{6}$$

Here, Q_e is the dimensionless Mie extinction efficiency factor, which is a function of particle radius r, wavelength λ, and the wavelength-dependent refractive index m_λ. Values of Q_e are computed from Mie theory using the complex refractive indices listed in Table 1.

[10] The LUT algorithm precomputes aerosol extinction at each of the SAGE II and CLAES wavelengths using equation (6). This is done for a range of unimodal lognormal size distributions $dN(r)/dr$ that are calculated by varying the parameters σ_g and R_{eff} in equation (1) (using equation (5) to relate R_{eff} and r_g). Specifically, σ_g is varied between 1.1 and 3.4 in steps of 0.1, while R_{eff} is varied from 0.1 to 2.0 μm in steps of 0.1 μm.

[11] In order to remove the dependence on total number of particles N_o in equation (1), the LUT computes ratios of the extinction $\beta(\lambda)$ at each wavelength λ to the extinction $\beta(\lambda_o)$ at a reference wavelength λ_o (i.e., $\beta(\lambda)/\beta(\lambda_o)$). This eliminates the need to solve for N_o, and leaves only two fitting parameters: σ_g and R_{eff}. The reference wavelength λ_o is chosen as the wavelength at which the SAGE II measurements have the smallest associated uncertainty within a sample bin. (This is discussed in detail in section 8.) This method is especially suited to retrieving R_{eff} because, as shown in equation (2), R_{eff} is equal to the ratio of the third to the second moment of the size distribution and hence is independent of N_o.

[12] The theoretical extinction ratios computed at each wavelength, and at each value of σ_g and R_{eff} in the above range, constitute the aerosol look-up table that is the basis for this retrieval algorithm. Figure 1 shows a sample graphical representation of the LUT. The figure shows the precomputed ratios $\beta(\lambda)/\beta(\lambda_o)$ when λ_o = 0.385, 0.453, 0.525 and 1.02 μm. The ratios are presented as a function of R_{eff} for four values of distribution widths in the range of values implemented by the LUT. Each colored line is the ratio of extinction at a given SAGE II or CLAES wavelength to the extinction at λ_o. It is interesting to note the significant variations in $\beta(\lambda)/\beta(\lambda_o)$ versus R_{eff} curves at smaller values of σ_g (narrower size distributions), compared to the monotonic behavior of the curves at larger σ_g.

3. Retrieval of Effective Radius

[13] The precomputed ratios exemplified by Figure 1 are compared with SAGE II and CLAES measurements of extinction or optical depth ratios (i.e., $\beta(\lambda)/\beta(\lambda_o)$ or $\tau(\lambda)/\tau(\lambda_o)$) to determine the range of R_{eff} consistent with the measured spectra and error bars for each σ_g value. Figure 2 is an example illustrating the LUT retrieval of R_{eff} for σ_g = 1.5. In this example, the reference wavelength is λ_o = 0.385 μm. On the right are the monthly-mean SAGE II and

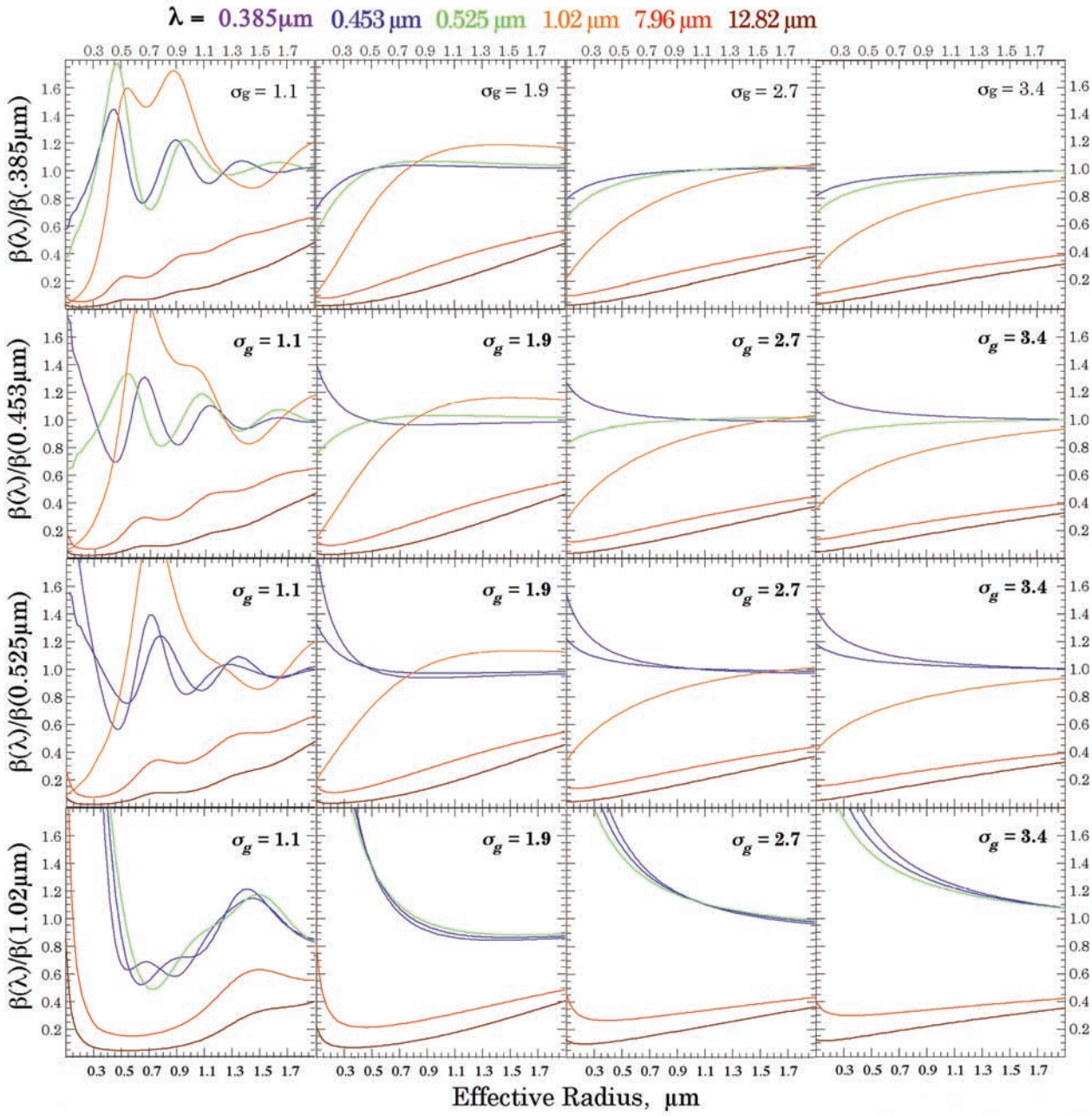

Figure 1. Calculated extinction ratios $\beta(\lambda)/\beta(\lambda_o)$ as a function of R_{eff} for σ_g = 1.1, 1.9, 2.7, 3.4. Each row represents values for a different reference wavelength λ_o.

CLAES measured optical depth ratios $\tau_m(\lambda)/\tau_m(\lambda_o)$ for February 1992 at 25–30°N. The measured error bars $\delta\ (\tau_m(\lambda)/\tau_m(\lambda_o))$ serve as the upper and lower limit on the corresponding precomputed ratios $\tau_p(\lambda)/\tau_p(\lambda_o)$ that are shown on the left as a function of R_{eff}. The light-colored horizontal bands in each frame highlight comparisons between the measured optical depth ratios on the right and the precomputed ratios on the left. The gray region in each frame marks the range of R_{eff} consistent with the measured spectrum. Values of R_{eff} are excluded from the solution range if the corresponding precomputed ratios $\tau_p(\lambda)/\tau_p(\lambda_o)$ differ from the measured ratios $\tau_m(\lambda)/\tau_m(\lambda_o)$ by more than $\delta\ (\tau_m(\lambda)/\tau_m(\lambda_o))$. The dark-colored bars along the abscissa serve to emphasize the solution region.

[14] Figures 2a–2d illustrate successively how the solution range narrows as measurements at additional wavelengths are used. For example, Figure 2a shows that if the only measurements considered are those at the two shortest SAGE II wavelengths, then the best estimate of R_{eff} is $R_{eff} \geq$ 0.28 μm. The solution range is highlighted by the gray region and dark-blue bar at the bottom of Figure 2a. In this limiting case, there is no upper bound on retrieved effective radius. Figure 2b extends the wavelength range to include the SAGE II ratio τ(0.525 μm)/τ(0.385 μm). This narrows the size range to $R_{eff} \geq$ 0.34 μm. However, the solution is

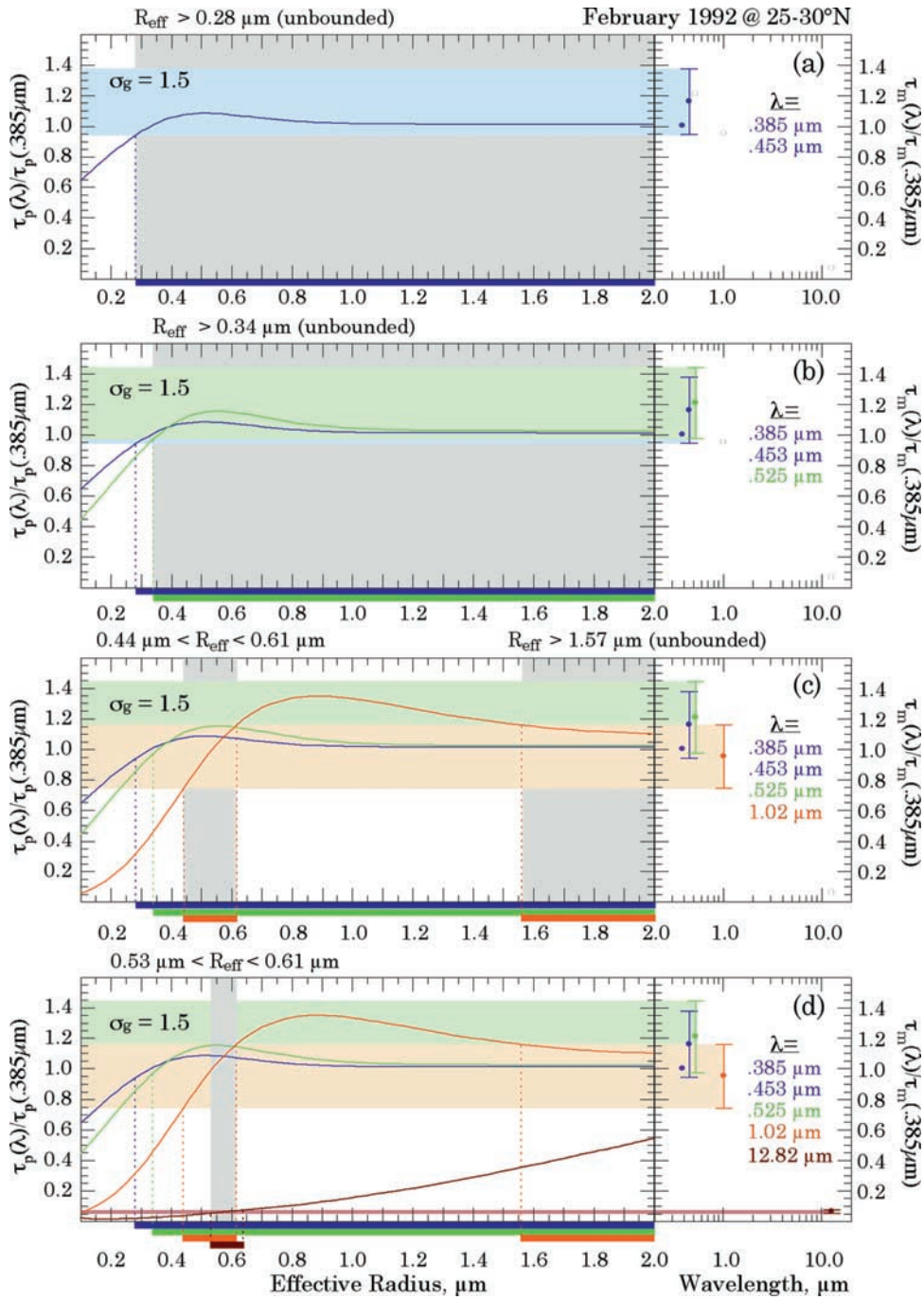

Figure 2. LUT retrieval of R_{eff} for $\sigma_g = 1.5$. On the right are the monthly mean measured optical depth ratios ($\tau(\lambda)/\tau(0.385\ \mu m)$) for February 1992 at 25–30° N. On the left are the corresponding calculated ratios as a function of R_{eff}. The light gray region in each frame marks the range of R_{eff} consistent with the measured spectrum. Figure 2a shows the retrieval technique when only the two shortest SAGE II wavelengths are employed. Figures 2b through 2d illustrate how the range of retrieved R_{eff} is narrowed by adding more wavelengths. The range of retrieved R_{eff} reflects both the values and uncertainties ("error bars") of measured optical depth ratios, propagated through the LUT curves of $\tau(\lambda)/\tau(0.385\ \mu m)$ versus R_{eff}.

still unbounded. Inclusion of the SAGE II 1.02 μm measurement in Figure 2c splits the R_{eff} solution into two ranges: 0.44 μm $\leq R_{eff} \leq$ 0.61 μm; and $R_{eff} \geq$ 1.57 μm. For this case (a post-Pinatubo volcanic spectrum), the retrieved estimate of R_{eff} using only the four SAGE II optical depths still has no upper limit. The retrieved range of R_{eff} is unbounded when the measured optical depth spectrum is flat within error bars, as is the case for the SAGE II wavelengths in this example.

[15] Spectrally flat extinction spectra in the near-UV to near-IR occur when R_{eff} exceeds ~0.5 μm. Putting an upper limit on the particle size requires adding information, for

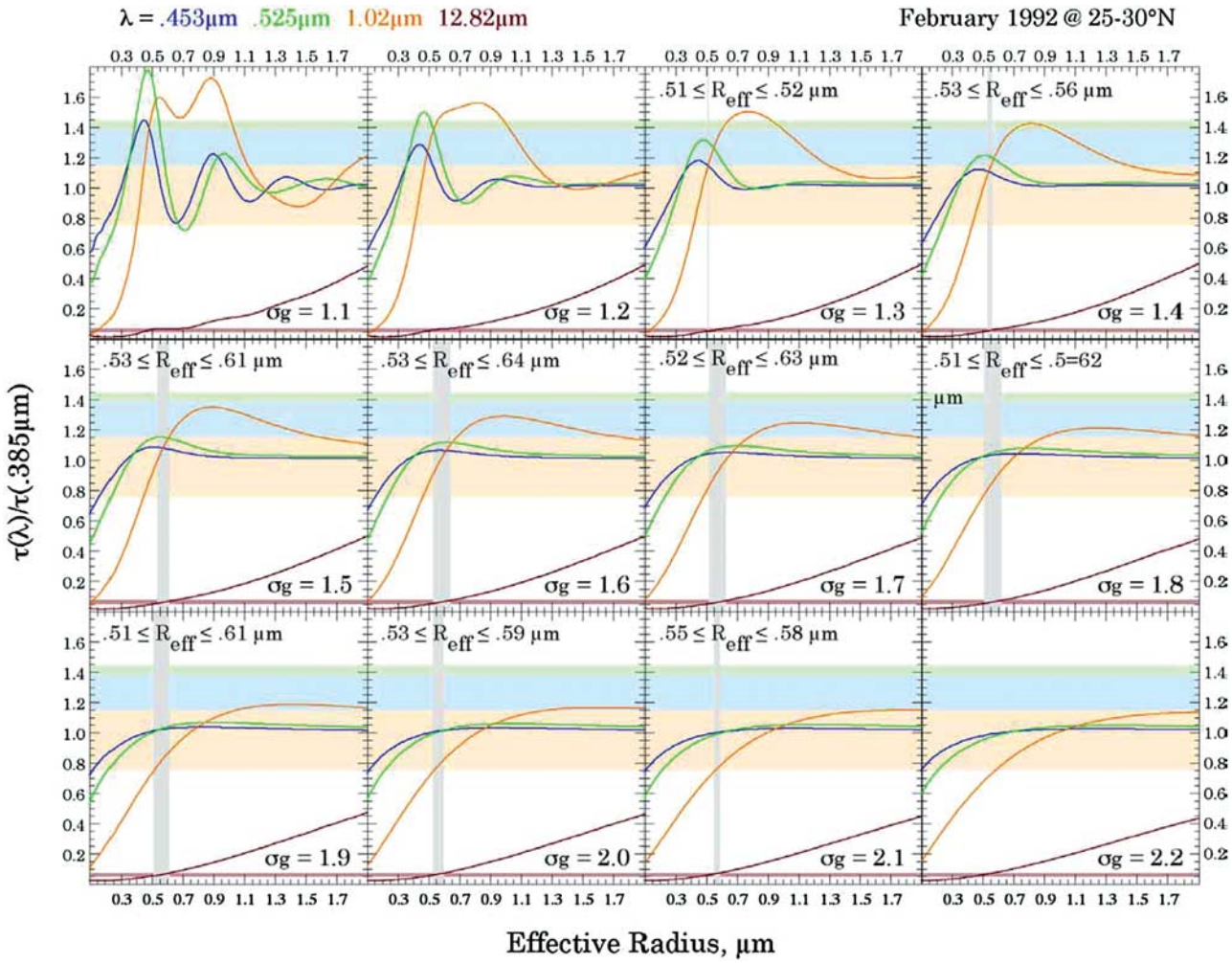

Figure 3. LUT retrieval of R_{eff} using a range of distribution widths for February 1992 at 25–30° N.

example by extending the measured optical depth spectrum further into the infrared. This is done in Figure 2d, which includes the ratio of the CLAES 12.82 μm optical depth to the optical depth at 0.385 μm (i.e., τ(12.82 μm)/τ(0.385 μm)). Using the full wavelength range of the SAGE II and CLAES composite, the retrieved estimate of effective radius for $\sigma_g = 1.5$ is $R_{eff} = 0.57 \pm 0.04$ μm.

[16] The above example illustrates how the LUT technique propagates measurement errors in optical depth to corresponding errors in retrieved R_{eff} (and analogously, to errors in retrieved S and V as discussed in section 6 below). The retrieval of R_{eff} in the above example was based on a single value of the size distribution width, $\sigma_g = 1.5$. Because the width of the actual size distribution is not known, the LUT algorithm allows σ_g to vary over a wide range, from 1.1 to 3.4, as illustrated in Figure 1. Without further information on σ_g, the overall solution range is determined by the maximum and minimum possible values of R_{eff} when all values of σ_g are considered. Figure 3 depicts the retrieval of R_{eff} for each value of σ_g using the same measured spectrum and technique as in Figure 2. As in Figure 2, the light-colored horizontal bands in each frame mark the upper and lower limit of the SAGE II and CLAES ratios. The retrieved range of R_{eff} for each value of σ_g is indicated by the vertical gray region and written at the top of each frame. In this example, the LUT is unable to retrieve solutions for values of $\sigma_g = 1.1$, 1.2 and $2.2 \leq \sigma_g \leq 3.4$. (Retrievals for $\sigma_g \geq 2.3$ are not shown for sake of brevity, but are similar to the retrieval at $\sigma_g = 2.2$, in that there are no solutions using the LUT technique.) For these distribution widths, there are no values of R_{eff} that are consistent with the measurements at all wavelengths using the LUT method. The retrieved range of R_{eff} based on the values of σ_g for which the LUT produces a solution is $0.51\ \mu m \leq R_{eff} \leq 0.64\ \mu m$. This is slightly larger than the previous range based solely on $\sigma_g = 1.5$.

[17] In certain situations, it is possible that for a given value of σ_g, the LUT technique produces a bifurcated solution for R_{eff}. That is, there can be two or more distinct ranges of R_{eff} that are consistent with the measured optical depth ratios. It is also possible that the largest retrieved R_{eff} range is unbounded. Solution bifurcation occurs because the Mie extinction efficiencies Q_e (and therefore the precalculated extinction ratio curves) are not a monotonic function of effective radius in the size range $0.1\ \mu m \leq R_{eff} \leq 2\ \mu m$. This is particularly true at the SAGE II wavelengths and for small values of σ_g (compare Figure 1). Oscillations in Mie extinction efficiencies are smoothed as the size distribution width σ_g is increased. Thus optical depth ratios produced for large σ_g values approach a monotonic function of particle

size. Optical depth ratios are also monotonic at the longer CLAES wavelengths (except for very small values of R_{eff}). As a result, solution bifurcation occurs most often when the SAGE II data are used exclusively, and for small values of the size distribution width. In the example given above, there are no values of σ_g that produce a bifurcated solution. However, had the CLAES data not been available in the above example, Figure 2c shows that the LUT would produce an unbounded, split range of R_{eff} for σ_g = 1.5. Solution bifurcation only occurred in 0.12% of our retrievals, calculated over the period 1985–1999 (which included CLAES data from January 1992 through May 1993). It should be pointed out that bifurcation of R_{eff} can also occur when combining R_{eff} solution ranges from the various values of σ_g used by the LUT algorithm. This produces solution bifurcation in less than 0.001% of the full range of data used in this study.

[18] Neither solution bifurcation, nor the inability of the LUT technique to retrieve a value of R_{eff} for a given value of σ_g, is sufficient to conclude that a particular distribution width is inconsistent with the measured optical depths. Should a given value of σ_g fail to retrieve a bounded range of R_{eff} that is not bifurcated, an alternative method of searching for a value of R_{eff} consistent with the measurements is implemented. This is discussed in section 5.

4. Distribution Width Criterion

[19] As mentioned above, the actual particle size distribution width is not known a priori. However, the LUT algorithm can retrieve some information about the distribution width by noting the range of σ_g values for which computed extinction spectra are consistent with the SAGE II and CLAES measurements. In the previous example, the LUT was able to return solutions of R_{eff} for the range $1.3 \leq \sigma_g \leq 2.1$ (Figure 3). Each σ_g value that returns a solution, together with the retrieved value of R_{eff}, is used to calculate optical depth $\tau_c(\lambda)$ at the SAGE II and CLAES wavelengths via equations (1) and (6). The total number of particles N_o in equation (1) is varied to obtain a best fit between the LUT-calculated optical depth spectrum $\tau_c(\lambda)$ and the measured spectrum $\tau_m(\lambda)$. The measure of consistency between computed and measured optical depth spectra is the quantity χ^2, defined by [*Bevington*, 1969]:

$$\chi^2 = \sum_{\lambda} \frac{(\tau_m(\lambda) - N_o\tau_c(\lambda))^2}{\delta_\lambda^2} \tag{7a}$$

Here, δ_λ is the uncertainty in the measurement $\tau_m(\lambda)$, and $\tau_c(\lambda)$ is the computed optical depth spectrum for N_o = 1. Note that N_o is written as a premultiplier to $\tau_c(\lambda)$ to emphasize the fact that it is used as a fitting parameter in determining the best fit spectrum. The criterion we used to determine which computed spectra are consistent with the measured spectrum is that χ^2 must be less than or equal to the number of measurement wavelengths. That is,

$$\chi^2 \leq \text{Number of Wavelengths.} \tag{7b}$$

Hence the average (over all wavelengths) of the squared difference between measured and calculated values (in units of measurement uncertainty) is required to be less than or equal to one. Thus our criterion is equivalent to the rule of thumb [e.g., *Bevington and Robinson*, 1992] that a fit is reasonable if χ^2/n is less than or "reasonably close to 1," if we take the number of wavelengths to be the number of degrees of freedom, n.

[20] The χ^2 criterion is illustrated in Figure 4 for the example given in the previous section (i.e., February 1992 at 25–30° N). The right hand panel gives values of χ^2 as a function of total number density N_o for the range of σ_g values that returned solutions of R_{eff}. The values of N_o that minimize χ^2 for each value of σ_g are used to compute the optical depth spectra shown on the left (colored dots). Also shown at left is the measured SAGE II and CLAES optical depth spectrum (black circles and error bars). The inset table lists the fitting parameters (σ_g and R_{eff}) for the computed spectra, and the corresponding minimum χ^2 value for each σ_g-R_{eff} pair. The best fit between the measured and calculated spectra occurs when the value of χ^2 is a minimum. In this example, the best fit spectrum occurs for σ_g = 1.6 and R_{eff} = 0.583 μm (marked by an asterisk in the inset table).

[21] It should be mentioned that there is an analytical solution for N_o, obtained by setting the derivative of equation (7a) with respect to N_o equal to zero, as follows:

$$\frac{\partial\chi^2}{\partial N_o} = 0 = \sum_{\lambda} \frac{2N_o\tau_c^2(\lambda) - 2\tau_m(\lambda)\tau_c(\lambda)}{\delta_\lambda^2} \tag{8a}$$

Solving equation (8a) for N_o yields:

$$N_o = \frac{\sum_\lambda \tau_m(\lambda)\tau_c(\lambda)/\delta_\lambda^2}{\sum_\lambda \tau_c^2(\lambda)\delta_\lambda^2} \tag{8b}$$

Values of N_o obtained analytically by equation (8b) agree to within 0.5% of the numerically-derived values of N_o depicted in Figure 4.

[22] Figure 4 shows that the value of χ^2 for σ_g = 2.1 is greater than the number of wavelengths - in this example, there are five measurement wavelengths. The maximum allowed value of χ^2 is depicted in the right frame by the horizontal dashed line. For σ_g = 2.1 and R_{eff} = 0.564 μm, there are no values of N_o that satisfy $\chi^2 \leq 5$. This suggests that this σ_g-R_{eff} pair is not consistent with the measurements. However, as in the case of solution bifurcation discussed in the previous section, should a given σ_g-R_{eff} pair not comply with the χ^2 criterion, an alternative method of searching for a value of R_{eff} consistent with the measurements is implemented, as discussed in the following section.

5. Parameter Search Technique

[23] For certain values of the size distribution width σ_g, the LUT technique is unable to retrieve a single, bounded range of R_{eff} that complies with the χ^2 criterion using the procedure illustrated by Figures 2 and 3. This, however, does not exclude a value of σ_g from being a suitable measure of the aerosol distribution width. For such values of σ_g, an alternative approach to searching for a value of effective radius consistent with the measurements is implemented. The parameter search technique (PST) varies R_{eff} and N_o to obtain computed spectra $\tau_c(\lambda)$ that fit the measured spectrum $\tau_m(\lambda)$ within our χ^2 criterion (7b).

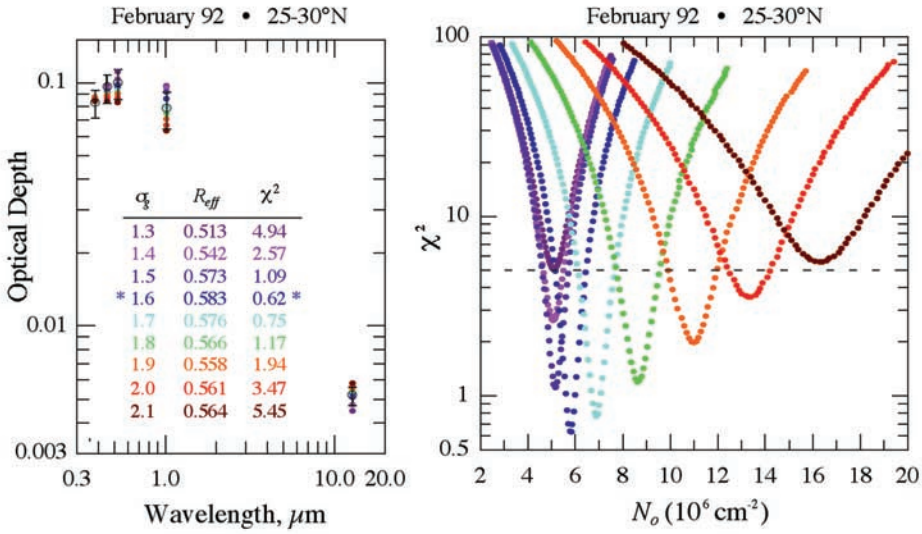

Figure 4. Left frame: Measured SAGE II and CLAES optical depth spectrum for February 1992 at 25–30° N (black circles and error bars) and the LUT-computed spectra for various values of σ_g (colored dots). The inset table lists the fitting parameters (σ_g and R_{eff}) for the computed spectra, and the corresponding minimum value of χ^2 determined by comparing the measured optical depth spectrum with those calculated by the LUT for a given σ_g-R_{eff} pair. Right frame: Computed χ^2 as a function of total number density N_o for the values of σ_g in the left frame.

[24] In the example given in the previous section, the LUT technique could not retrieve solutions for $\sigma_g = 1.1$, 1.2 and the range $2.2 \leq \sigma_g \leq 3.4$. In addition, the retrieval at $\sigma_g = 2.1$ is not compliant with the χ^2 criterion (equation (7b)). Figure 5 illustrates the results of applying the PST to each of these σ_g values to determine if any values of R_{eff} are consistent with measurements. Each frame in the figure applies to the value of σ_g printed in the upper right corner. (For the sake of brevity, results are not shown for $\sigma_g \geq 2.5$, which are similar to those for $\sigma_g = 2.4$.) The black dots and error bars repeated in each frame are the measured optical depths $\tau_m(\lambda)$ and uncertainties $\delta(\tau_m(\lambda))$, while the red dots are the best fit spectrum $\tau_c(\lambda)$ calculated from the indicated fitting parameters; σ_g, R_{eff} and N_o. The inset plots show corresponding values of χ^2 obtained by comparing the measured spectrum with spectra calculated for the range of effective radii shown on the x axis (i.e., equation (7a)). The value of R_{eff} that minimizes χ^2 for the indicated value of σ_g is used to compute the optical depth spectrum $\tau_c(\lambda)$ shown in each frame. The χ^2 criterion presented in the previous section (i.e., $\chi^2 \leq 5$) is imposed on the PST results. The dashed horizontal line on the inset plots in Figure 5 shows the maximum allowed value of χ^2. Of the distribution widths shown in Figure 5, the only ones to satisfy this constraint are $\sigma_g = 2.1$, 2.2 and 2.3. The remaining values of σ_g (i.e., $\sigma_g = 1.1$, 1.2, and $2.4 \leq \sigma_g \leq 3.4$) have no computed spectra that meet our χ^2 criterion (7b).

[25] It is interesting to note that the LUT originally retrieved a value of $R_{eff} = 0.564$ μm for $\sigma_g = 2.1$ (Figures 3 and 4) that did not satisfy the χ^2 criterion (7b). The PST then found for this distribution width a slightly smaller value of $R_{eff} = 0.49$ μm that has a corresponding value of $\chi^2 \leq 5$. Also, the LUT technique was originally unable to retrieve any allowed values of R_{eff} for $\sigma_g = 2.2$ and 2.3, but the PST subsequently found values of R_{eff} that satisfy the χ^2 criterion (equation (7b)) for both distribution widths. Note that the χ^2 criterion allows the optical depth $\tau_c(\lambda)$ calculated at a given wavelength to differ from the corresponding measured optical depth $\tau_m(\lambda)$ by more than $\delta(\tau_m(\lambda))$ (as in the Figure 5 for $\sigma_g = 2.3$ at 1.02 μm) provided $\chi^2 \leq 5$. In contrast, the LUT procedure illustrated in Figures 2 and 3 excludes values of R_{eff} if even a single precomputed ratio $\tau_p(\lambda)/\tau_p(\lambda_o)$ differs from $\tau_m(\lambda)/\tau_m(\lambda_o)$ by more than $\delta(\tau_m(\lambda)/\tau_m(\lambda_o))$.

[26] The overall retrieved range of σ_g for which either the LUT or PST produces an acceptable solution is $1.3 \leq \sigma_g \leq 2.3$. On the basis of this σ_g range, the retrieved range of R_{eff} is $0.45\ \mu m \leq R_{eff} \leq 0.64\ \mu m$ (Figures 3 and 5). The lower limit of the R_{eff} range extends to slightly smaller particles than the lower limit of the range retrieved without applying the parameter search technique. The best fit estimate of R_{eff} based on calculations of χ^2 is still $R_{eff} = 0.583$ μm for $\sigma_g = 1.6$.

[27] Retrievals of R_{eff} and σ_g that make up the data set presented in paper 2 are based on the above procedures. For example, for February 1992 at 25–30°N, the reported value of σ_g is 1.6 ± 0.5 while the reported value and range of R_{eff} are those obtained using both the LUT and PST techniques (i.e., best fit $R_{eff} = 0.583$ μm, allowed range 0.45 to 0.64 μm). Note that when the remaining sections refer to retrievals by the LUT algorithm, it is understood that the PST technique was used when the LUT algorithm did not return any σ_g - R_{eff} pairs meeting the χ^2 criterion. Also included in our results are retrievals of particle surface area S and volume V, the derivation of which is presented below.

6. Retrieval of Surface Area and Volume

[28] Estimates and uncertainties of total particle surface area S and volume V are derived from retrieved values of the

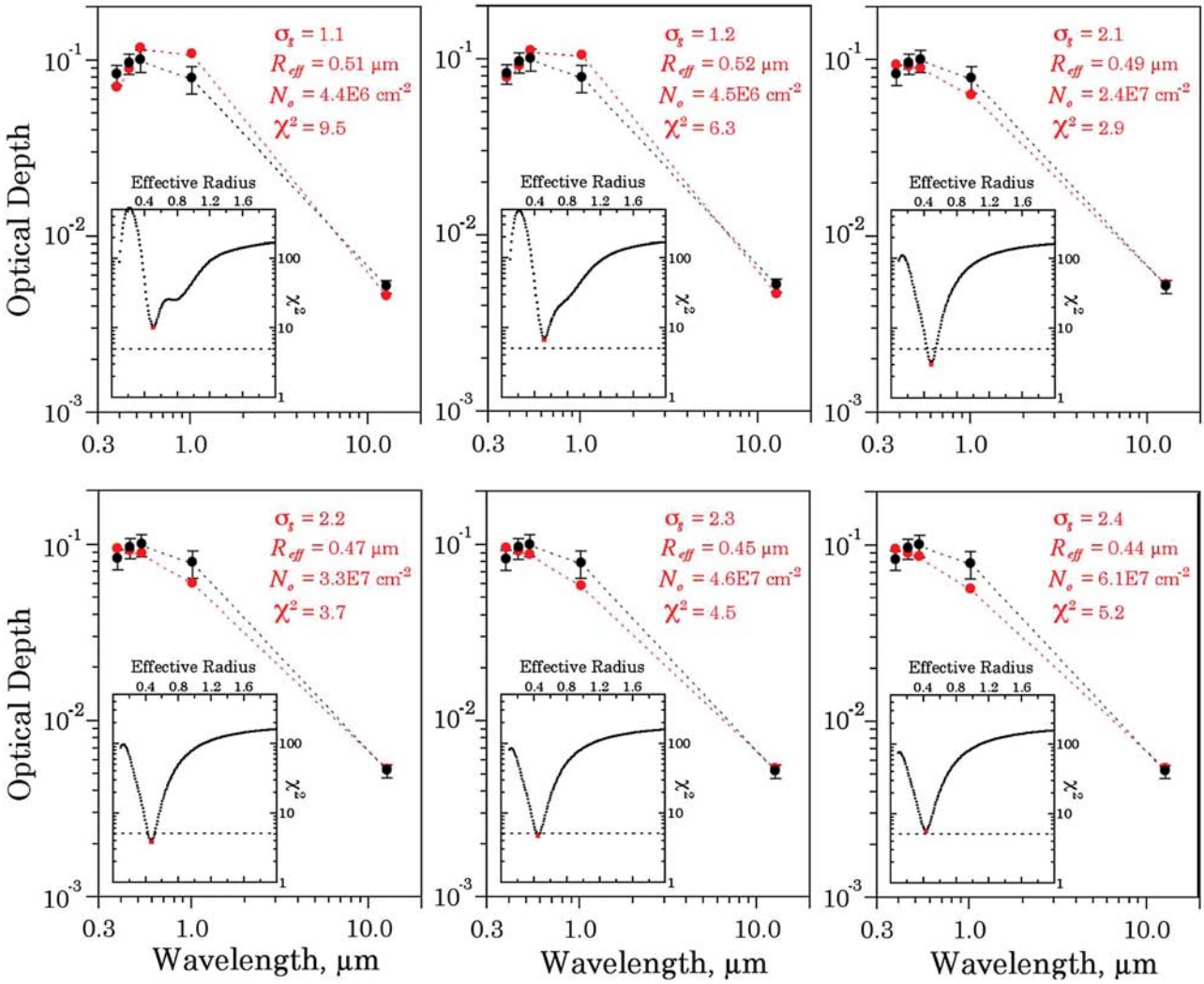

Figure 5. Parameter search technique PST for February 1992 at 25–30°N. Each frame represents the results of applying the PST technique to a given value of σ_g. The black dots and error bars are the measured spectrum and uncertainties, while the red dots are the best fit spectrum calculated from the fitting parameters in the upper right corner. The inset plots show corresponding χ^2 values obtained by comparing the measured spectrum with spectra calculated for the range of effective radii shown on the x axis. The horizontal dashed line marks the maximum allowed value of $\chi^2 = 5$.

size distribution fitting parameters σ_g, R_{eff} and N_o. Each retrieved set of parameters is used to calculate $dN(r)/dr$ via equation (1). Estimates of $dN(r)/dr$ are then used to determine aerosol surface area and volume distributions as follows

$$\frac{dS}{d\ln r} = 4\pi r^2 \frac{dN(r)}{d\ln r} \tag{9a}$$

$$\frac{dV}{d\ln r} = \frac{4\pi}{3} r^3 \frac{dN(r)}{d\ln r} \tag{9b}$$

[29] Figure 6 shows examples of $dS(r)/d\ln r$ (left frame) and $dV(r)/d\ln r$ (right frame) as a function of particle radius for each allowed value of σ_g for February 1992 at 25–30°N. The table lists the values of σ_g and the corresponding column values of integrated S and V. Using a range of distribution widths enables the retrieval technique to put error limits on estimates of S and V. Specifically, the technique reports the mean and standard deviation of the values of S and V retrieved for the range of allowed σ_g values. In the example given, the reported values of S and V based on the σ_g range listed in the table are $S = (1.31 \pm 0.08) \times 10^7$ $\mu m^2 cm^{-2}$ and $V = (2.33 \pm 0.10) \times 10^6$ $\mu m^3 cm^{-2}$.

[30] A relationship between S and V, and the second and third moments of the size distribution, respectively, is established by integrating equations (9a) and (9b). Equation (2) can then be used to derive an expression for particle effective radius in terms of the total volume and surface area as follows:

$$R_{eff} = 3V/S \tag{10}$$

Retrievals of R_{eff} from the LUT algorithm can be compared with estimates of R_{eff} based on equation (10). For example, using the above retrievals of S and V in equation (10) yields

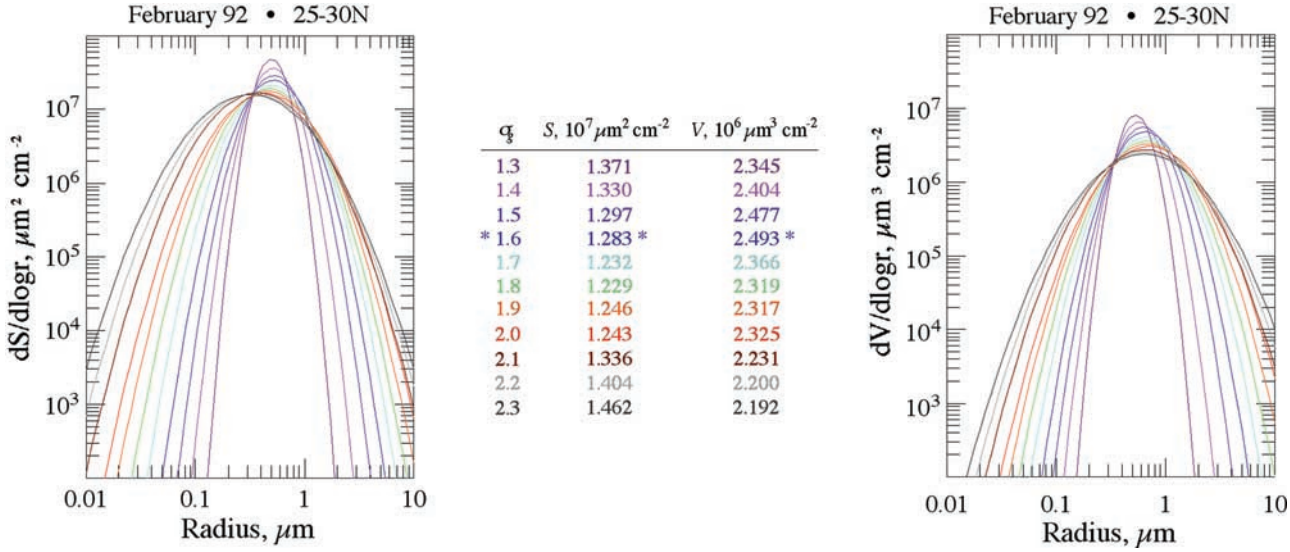

σ_g	S, $10^7\,\mu m^2\,cm^{-2}$	V, $10^6\,\mu m^3\,cm^{-2}$
1.3	1.371	2.345
1.4	1.330	2.404
1.5	1.297	2.477
* 1.6	1.283 *	2.493 *
1.7	1.232	2.366
1.8	1.229	2.319
1.9	1.246	2.317
2.0	1.243	2.325
2.1	1.336	2.231
2.2	1.404	2.200
2.3	1.462	2.192

Figure 6. Retrieved column surface area (left frame) and volume distributions (right frame) as a function of distribution width σ_g for February 1992 at 25–30°N. Retrievals are shown for values of σ_g that return solutions of R_{eff} using the LUT and PST techniques. The inset table lists the values of σ_g and the corresponding estimates of integrated S and V.

$R_{eff} = 0.536$ μm. This value is slightly smaller than the best fit estimate of $R_{eff} = 0.583$ μm using the LUT algorithm, but identical to the mean of the R_{eff} values in Figures 4 and 5 (i.e., 0.536 μm).

[31] Estimates of particle volume V can also be calculated by applying extinction-to-volume ratios (which we can assume to be 7.51×10^{-4} $cm^3\mu m^{-3}$ km^{-1} at 7.96 μm, and 1.52×10^{-4} $cm^3\mu m^{-3}$ km^{-1} at 12.82 μm [*Livingston*, 1996]) directly to the CLAES 7.96 μm and 12.82 μm extinction measurements. Estimates of volume based on these extinction-to-volume ratios provide a straightforward method of checking the LUT retrievals of volume.

7. Bias Due to Assumption of Unimodality

[32] As noted in section 2, the LUT algorithm assumes a unimodal lognormal functional form to describe the stratospheric aerosol. *Pueschel et al.* [1989] and *Goodman et al.* [1994] state that this approximation is well suited for nonvolcanic stratospheric aerosols. It has been used extensively in previous investigations to describe distribution shape [e.g., *Yue and Deepak*, 1983, 1984; *Wang et al.*, 1989; *Russell et al.*, 1993b; *Yue et al.*, 1994; *Kent et al.*, 1995]. However, both volcanic and nonvolcanic distributions are often bimodal. For example, *Deshler et al.* [1993] measured vertical profiles of the Pinatubo aerosol from June 1991 to January 1993, and concluded that aerosol size distributions during this period are well characterized using bimodal lognormal distributions at altitudes below 22 km. They state that above this altitude unimodal distributions are adequate. In situ data from *Deshler and Oltmans* [1998] and T. Deshler (University of Wyoming, personal communications, 1999) show that two modes are often required to fit particle distributions measured in 1997–1999, a period considered near-background. This raises the question of whether the assumption of unimodality in the LUT can introduce bias and/or uncertainty into retrieved values of R_{eff}, S and V.

[33] Some properties of the aerosol depend on characteristics of the size distribution at one extreme or the other. Examples are the mean radius, total particle number, and high-order moments (M_n, $n \geq 4$). *Thomason and Poole* [1993] point out that estimates of such quantities are highly dependent on a priori assumptions about the shape of the distribution. (In fact, parameter retrieval may be more sensitive to the assumed form of size distribution than to uncertainty in the measured extinction [*Ben-David et al.*, 1988].) Assessing the bias in retrieved aerosol quantities thus requires an understanding of how accurately unimodal distributions can describe the large- and small-particle modes of the "true" distribution over a range of stratospheric conditions. *Russell et al.* [1996] concluded that retrieved unimodal distributions accurately described the second, larger mode of several post-Pinatubo bimodal size distributions measured between August 1991 and February 1992, but failed to account for the smaller particles in the first mode. This is reasonable when the larger particle mode dominates extinction and $dS(r)/dr$, as occurred 1 to 2 years after the Pinatubo eruption. In these conditions, smaller particles contribute little to the measured extinction spectra (for $\lambda > 0.385$ μm). It was shown by *Thomason* [1991] that extinction measurements in the SAGE II spectral region have little sensitivity to particles with radius smaller than 0.1 μm. Measurements at shorter wavelengths would enhance the sensitivity to smaller particle sizes. Unfortunately, strong O_3 absorption in the lower stratosphere prohibits accurate aerosol extinction measurements by solar occultation methods below a wavelength of about 0.3 μm. The contribution of such small particles to total extinction at the SAGE II wavelengths generally falls within the experimental error associated with the measurements and the retrieval algorithm. SAGE II measurements do not have the measurement accuracy or spectral range to retrieve six fitting parameters of a bimodal lognormal distribution (i.e., σ_g^1, R_{eff}^1, N_o^1, σ_g^2, R_{eff}^2, N_o^2). For this

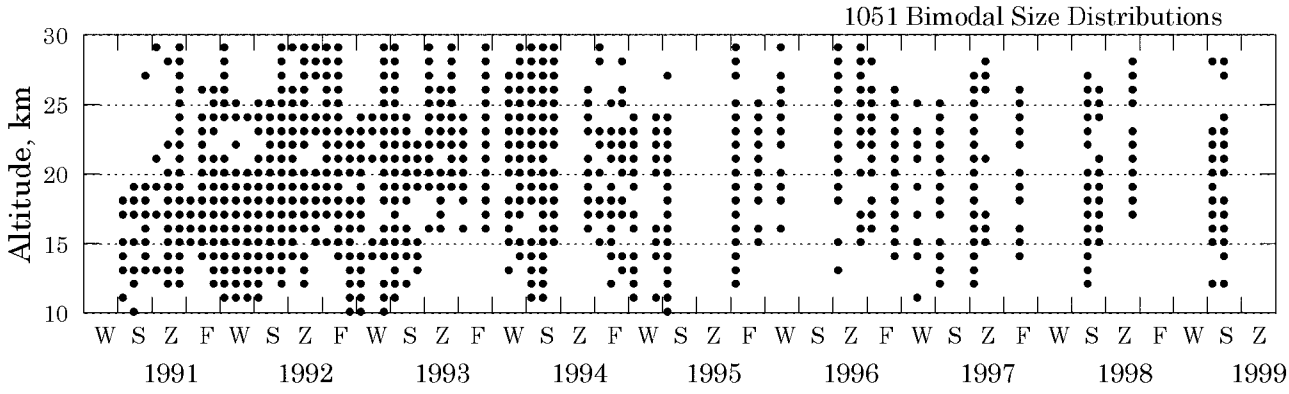

Figure 7. Altitude and time of measured bimodal size distributions from *Deshler et al.* [1993], *Deshler and Oltmans* [1998], *Pueschel et al.* [1992, 1994], and *Goodman et al.* [1994].

reason, the LUT algorithm assumes a unimodal lognormal distribution.

[34] A procedure to estimate and remove any bias caused by assuming a unimodal functional form is incorporated into the LUT algorithm. The bias is determined by testing the algorithm's performance with synthetic extinction spectra calculated from bimodal size distributions obtained from airborne wire-impactor and balloon-borne dustsonde measurements that approximately coincide in space and time with SAGE II and CLAES measurements. Several series of aircraft observations following Pinatubo were reported by *Pueschel et al.* [1992, 1994] and *Goodman et al.* [1994]. Unfortunately, they are limited to sampling once every few months, and to the lowest altitudes of the aerosol layer (from 18 to 19 km) over western North America. Dustsonde measurements reported by *Hofmann and Rosen* [1983] and *Deshler et al.* [1992, 1993] consist of regular observations of El Chichón and Pinatubo, but are limited to a temporal resolution of about one measurement profile per month on average. Similarly, these data only apply to a single location (normally over Laramie, Wyoming), although a few flights were made at other locations. *Oberbeck et al.* [1983] and *Knollenberg and Huffman* [1983] also report in situ aerosol size data following El Chichón. In general, data before 1991 are sparse, and they are not considered here. The altitudes of measurements used for this analysis are shown in Figure 7 as a function of time. Overall, there are 1051 bimodal distributions, 95% of which are from *Deshler et al.* [1993] and *Deshler and Oltmans* [1998]. Measurements extend from March 1991 to April 1999, and from 10 to 30 km. Distributions are split into four 5-kilometer altitude bands (i.e., 10–15 km, 15–20 km, . . ., 25–30 km) in order to estimate an altitude- and time-dependent bias correction. Bias correction is not applied above 30 km because, as mentioned above, unimodal lognormals are adequate for describing aerosol distributions at higher altitudes [*Deshler et al.*, 1993].

[35] *Bauman* [2000] carried out a detailed analysis of the effect of assuming a unimodal size distribution in the LUT when the actual distribution is bimodal. The procedure was to take measured bimodal size distributions and use them to generate synthetic extinction spectra. These spectra were then input to the LUT algorithm, which retrieved the best fit unimodal lognormal size distributions. We now describe the results of this study for two cases, one in which the large mode makes the dominant contribution to surface area S, and the other in which the small mode is the dominant contributor. In the case of large mode dominant bimodal distributions the retrieved unimodal size distribution matched the large mode of the bimodal size distribution quite well, but failed to account for the particles in the smaller mode. This was true even in cases when the two modes had nearly the same peak value of dS/dln r. Nevertheless, the extinction spectra returned by the LUT from the unimodal distribution were in all cases a very good fit to the synthetic spectra calculated from the measured bimodal size distributions. The failure of the LUT-retrieved unimodal distributions to account for the small mode caused the LUT to overestimate R_{eff} and underestimate S relative to values calculated directly from the input bimodal distributions. LUT retrievals also generally overestimated V, though by a smaller percentage than the overestimate in R_{eff} (consistent with the relationship of R_{eff}, V, and S in equation (10)).

[36] *Bauman* [2000] carried out the same analysis for small-mode-dominant bimodal distributions. In these cases the LUT retrieved unimodal distributions tended not to capture the large particle tail of the bimodal distributions.

Table 2. Bias Correction Coefficients[a]

	Effective Radius			Surface Area			Volume		
Altitude	A	B	r^2	A	B	r^2	A	B	r^2
25–30 km	4.44E-05	9.82E-02	3.46E-02	−3.30E-05	−1.39E-01	1.75E-02	−1.25E-04	2.97E-02	2.08E-01
20–25 km	3.61E-05	9.60E-02	3.08E-02	−8.12E-05	6.71E-02	1.02E-01	−1.31E-04	1.90E-01	2.68E-01
15–20 km	−2.46E-06	1.83E-01	1.41E-04	−9.10E-05	−1.41E-03	1.47E-01	−6.02E-05	1.95E-02	2.89E-02
10–15 km	−4.34E-05	1.89E-01	4.19E-02	−1.78E-05	−2.32E-01	8.24E-03	1.10E-05	−3.79E-02	1.27E-03

[a]The relative difference Δ between LUT-retrieved values of R_{eff}, S and V and those values calculated directly from measured bimodals is given by: $\Delta = A * d + B$, where d is the number of days since 15 June 1991. The fitted parameters A and B and the coefficients of determination r^2 are listed as a function of altitude band and retrieved parameter.

Table 3. Root-Mean-Square and Standard Deviation of the Relative Difference Between Retrieved and Assumed Values of R_{eff}, S, and V, as a Function of Altitude Band[a]

	Effective Radius		Surface Area		Volume	
Altitude	RMS	Σ	RMS	σ	RMS	σ
25–30 km	0.251	0.193	0.281	0.208	0.249	0.218
20–25 km	0.217	0.167	0.212	0.210	0.192	0.184
15–20 km	0.251	0.174	0.239	0.213	0.225	0.224
10– 15 km	0.265	0.184	0.265	0.177	0.205	0.205
Average	0.246	0.180	0.249	0.202	0.218	0.208

[a]RMS, root-mean-square; σ, standard deviation. Retrievals use synthetic extinction spectra calculated from measured size distributions, with no extinction error added.

Nevertheless, there was still a near perfect match between the extinction spectra of the bimodal and the retrieved unimodal size distributions. This indicates that when the small mode dominates S, very large particles (which are underrepresented in the LUT-retrieved unimodal distributions) contribute little to extinction in the SAGE II spectral region. As in the case of large-mode-dominant bimodal distributions, the LUT retrievals of R_{eff} are greater than those of the input bimodal distributions, while retrievals of S are less. However, retrievals of V tend to be less than the input bimodal values when the small mode dominates. This is consistent with equation (10) since the percentage difference between the input and retrieved values of S is usually larger than the difference between corresponding values of R_{eff}.

[37] It should be pointed out that it is difficult to measure a statistically significant number of large particles using in situ methods. Further, adiabatic heating of decelerating air can volatize particles entering or impacting in situ aircraft instruments, which leads to underestimates of particle size [*Pueschel et al.*, 1994]. Lognormal fits to in situ size distributions often have relatively large error bars on the large-particle tail of the distribution [*Russell et al.*, 1993a]. Such fits may not adequately describe measured distributions containing a significant number of large particles. Another potential source of error is that dustsonde instruments often measure more particles in the small-particle mode than do wire-impactor instruments. An underestimate in the number of small particles can also cause overestimates in calculations of effective radius. The majority of the bimodal distributions used in this analysis are dustsonde measurements, so the reader should be aware of these caveats.

[38] The difference between LUT-retrieved values of R_{eff}, S and V and values calculated directly from bimodal distributions is a measure of the error introduced into the LUT method due to the assumption of unimodality. Figure 8 shows the results of applying the above technique to each of the 1051 size distributions whose altitude and date are shown in Figure 7. Each successive frame presents a time series of the relative difference in retrievals of R_{eff}, S and V in one of the four specified altitude bands. (The altitude range is denoted in the top right corner of each frame.). The solid curves are linear fits to the data. In our final results these fits are subtracted from LUT retrievals to obtain bias-corrected retrievals. Curve fitting parameters are listed in Table 2 as a function of altitude band. Bias correction is applied to all results after 15 June 1991 presented in paper 2. Table 2 also lists "coefficients of determination" r^2 for each linear fit. r^2 is the fraction of the variance in Δ that is explained by the fitted line. The small values of r^2 show that time dependence explains little of the variance in bias due to assumption of unimodality.

[39] Table 3 lists the root-mean-square (RMS) and the standard deviation (σ) of the relative difference between retrieved and assumed values of R_{eff}, S and V shown in Figure 8 as function of altitude band. The values reflect the accuracy with which the LUT (prior to bias correction) is able to retrieve aerosol parameters from synthetic (i.e., error-free) measurements of extinction. The RMS value is the expected error in LUT retrievals before bias correction (again, for error-free extinction measurements). After bias correction, the uncertainty is reduced to the standard deviation. Bias correction reduces uncertainty in retrievals of R_{eff}, S and V by approximately 7%, 5% and 1%, respectively, averaged over all altitude bands. After bias correction is applied, the uncertainty in LUT retrievals is approximately ±20% for S and V, with slightly smaller values for R_{eff}. We emphasize that these uncertainties are for synthetic input extinction spectra with no uncertainty from measurement error or spatiotemporal variability. The propagation of the latter uncertainties into retrieved parameters is illustrated in Figure 2 and discussed further below.

8. Sensitivity to Aerosol Variability and Measurement Uncertainty

[40] The method by which average extinction and its uncertainty are calculated within a sample bin (i.e., 1 month × 5° latitude × 1 km altitude) is important since the error bars on input extinction measurements primarily determine upper and lower limits on retrieved particle size, area and volume. SAGE II and CLAES measurements are generally not coincident in space and time. Therefore atmospheric spatiotemporal variability must be taken into consideration when combining SAGE II and CLAES measurements to get a bin-averaged spectrum and its uncertainty. Instrument uncertainty must also be taken into account.

[41] The LUT sensitivity to different methods of accounting for atmospheric or sampling variability and measurement uncertainty within a month-latitude-altitude bin is examined in Figure 9. The symbols "R", "K", "H" and "P" indicate the time and geographic locations of eruptions of Ruiz, Kelut, Hudson and Pinatubo. The left frames are averaged extinction spectra and uncertainties for January 1991 and 1992 at 25.5 km and 15–20° N. Five alternative methods are used to compute averages and error bars (labeled a–e in the lower right corner of the leftmost

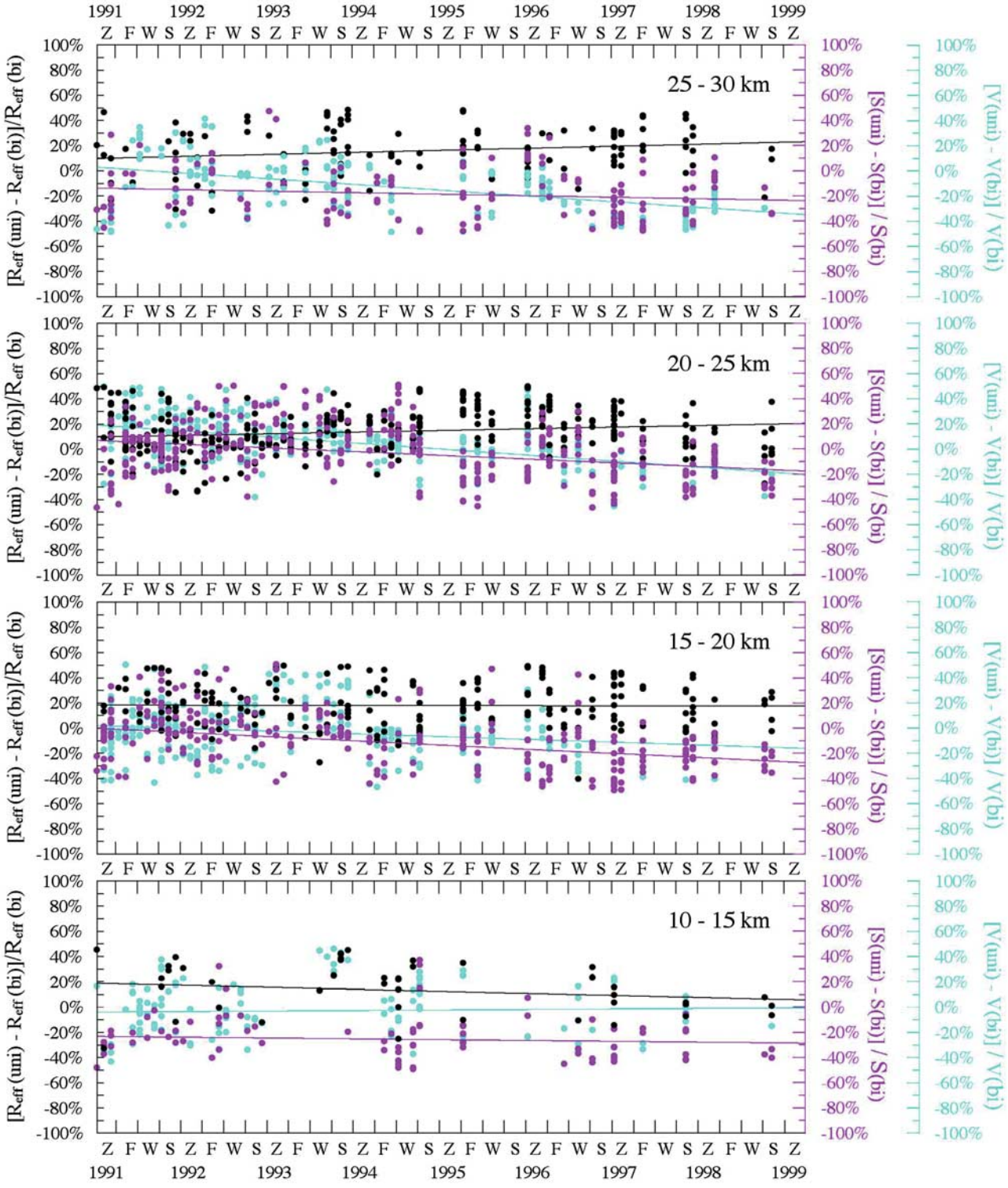

Figure 8. Results of applying the LUT algorithm to synthetic extinction spectra calculated from measured bimodal size distributions obtained from *Deshler et al.* [1993], *Deshler and Oltmans* [1998], *Pueschel et al.* [1992, 1994], and *Goodman et al.* [1994]. R_{eff}(bi), S(bi) and V(bi) are the effective radius, surface area and volume of the measured bimodal size distribution, and R_{eff}(uni), S(uni) and V(uni) are the corresponding values returned by the LUT using best fit spectra. The results for R_{eff} are on the left ordinate in black, and the results for S and V are on the right ordinate in pink and blue, respectively. The solid curves are linear fits to the data. Curve fitting parameters are listed in Table 2.

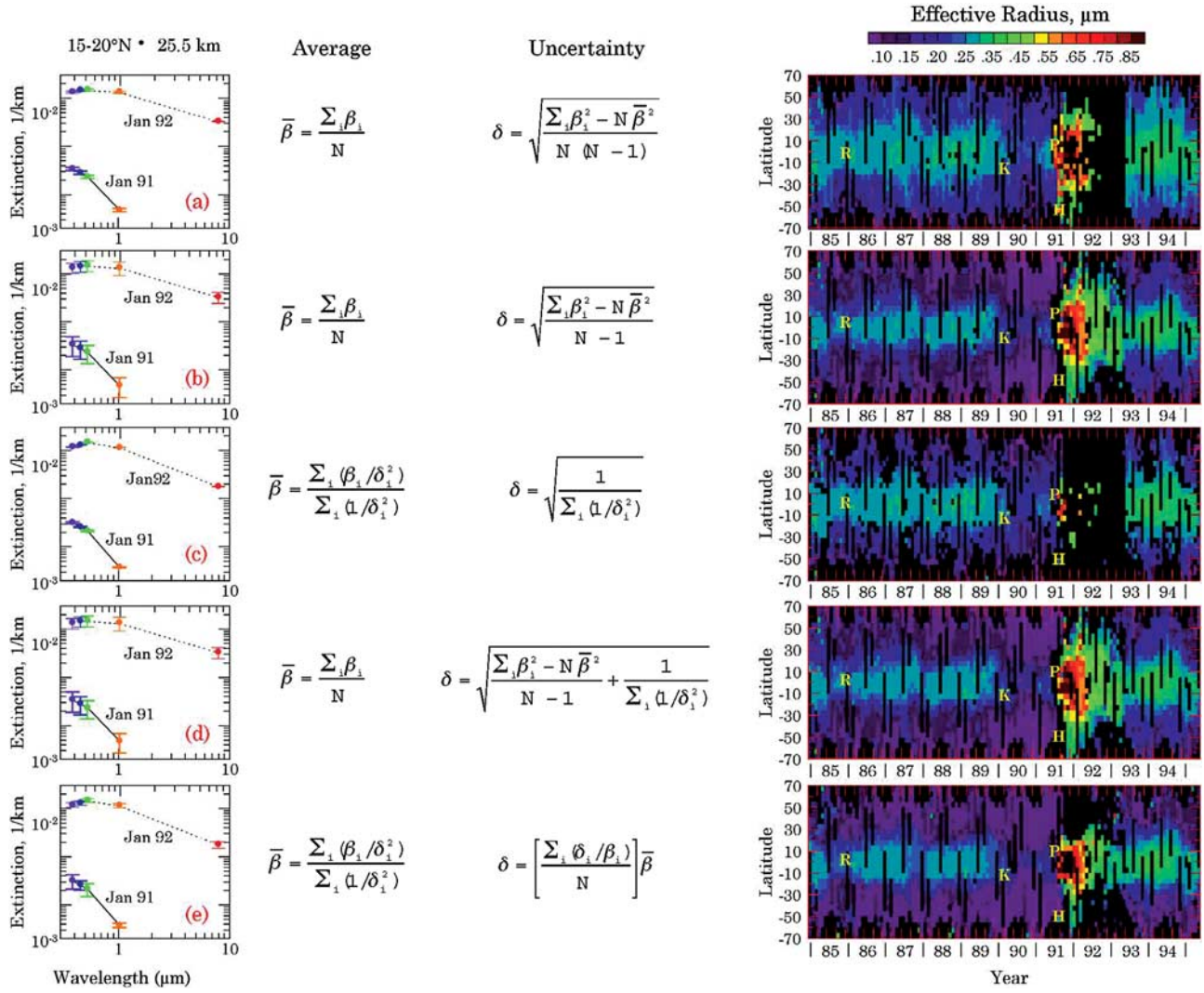

Figure 9. LUT sensitivity to different methods of accounting for atmospheric variability and measurement uncertainty. Left frames: Bin-averaged extinction spectra and uncertainties for January 1991 and 1992 at 25.5 km and 15–20°N. Five alternative methods are used to compute bin-averages and error bars (labeled a–e in the lower right corner of leftmost frames). Methods are shown in equations in the center, and correspond to: (a) mean and standard deviation of the mean; (b) mean and standard deviation of the population; (c) weighted mean and weighted uncertainty; (d) mean and combination of uncertainty in Figures 9b and 9c; and, (e) weighted mean and an estimate of the individual measurement error. Right Frames: Retrievals of R_{eff} as a function of latitude and time, based on spectra and uncertainties in the left frames.

frames). Methods are shown in equations in the center, and correspond to: (a) mean and standard deviation of the mean; (b) mean and standard deviation of the population; (c) weighted mean and weighted uncertainty; (d) mean and combination of uncertainty in Figures 9b and 9c; and, (e) weighted mean and an estimate of the individual measurement error. The right frames show retrievals of R_{eff} as a function of latitude and time, based on spectra and uncertainties in the left frames.

[42] The relative magnitudes of the error bars on the left are noticeably different for the five alternative methods. The largest error bars result from using the population standard deviation (Figures 9b and 9d). This suggests that aerosol variability within a bin dominates the error contribution from measurement uncertainty. The right frames of Figure 9 show that in certain situations, retrieval of R_{eff} is not possible if the error bars are too small. This is the case in the year or two following the eruption of Mount Pinatubo, particularly at high latitudes.

[43] The results presented in paper 2 use method (d) to determine the average extinction and uncertainty within a bin. This method considers both aerosol variability and measurement uncertainty, and enables the greatest occurrence of LUT retrievals. This latter point is important because it suggests that SAGE II and CLAES measurements are most consistent when both sources of uncertainty (i.e., spatiotemporal variations and measurement error) are taken into consideration when determining bin averages.

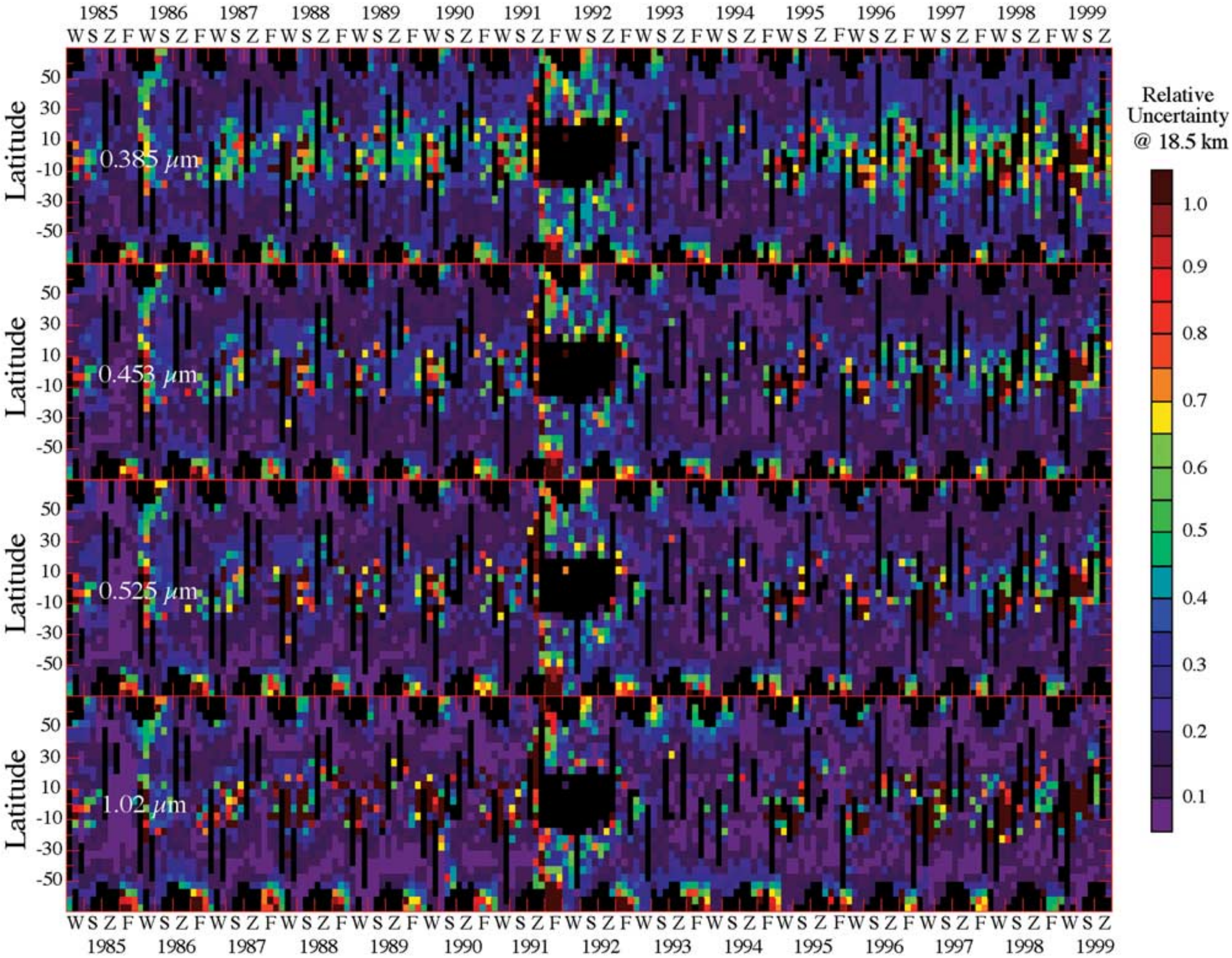

Figure 10. The average relative uncertainty of the binned SAGE II measurements at 18.5 km resulting from spatiotemporal variability and instrument uncertainty.

[44] We evaluated the average relative uncertainties (i.e., δ/β) in the CLAES and SAGE II measurements as a function of time and latitude at 18.5 and 25.5 km in each latitude/longitude bin. With few exceptions the CLAES relative uncertainties are in the 0 to 0.2 range. In the tropics at the lower altitude the winter-spring relative uncertainties are higher, about 0.4. At very high latitudes during the winter, values close to unity occur occasionally. The SAGE results are similar but exhibit higher uncertainties in the tropics with occasional values greater than 0.8. There are also large uncertainties at all latitudes for a year following the Pinatubo eruption. It is probable that the large SAGE II uncertainties in the tropics at 18.5 km result from variability in upper tropospheric cirrus clouds. An example of these results is presented in Figure 10, which gives the values of δ/β in the SAGE II measurements at 18.5 km. More extensive results for SAGE II and CLAES are presented by *Bauman* [2000].

9. Sensitivity to Refractive Index

[45] There are numerous publications [e.g., *Massie et al.*, 1996; *Grainger et al.*, 1995; *Liu et al.*, 1999] that suggest the assumed optical constants are one of the largest uncertainties in retrieving aerosol properties. Therefore the sensitivity of LUT retrievals to refractive index is examined here. This study was carried out to determine if the commonly used 300 K indices of refraction of *Palmer and Williams* [1975] give different results than the more recent *Tisdale et al.* [1998] values at 215 K. Table 1 lists estimates of the real and imaginary indices at the SAGE II and CLAES wavelengths used in this research. The indices from *Tisdale et al.* [1998] are determined for 215 K and are interpolated to 70.85% H_2SO_4 solution. We used 70.85% (by weight) sulfuric acid solutions because this is the expected composition of the stratospheric aerosol particles if one assumes a temperature of 215 K and an environmental water vapor mixing ratio of 3 ppmv [*Steele and Hamill*, 1981]. To match the *Tisdale et al.* [1998] indices in the infrared, the indices in Table 1 derived from *Palmer and Williams* [1975] include a Lorentz-Lorenz temperature correction from 300 K to 215 K and are interpolated to 70.85% H_2SO_4.

[46] Figure 11 compares LUT retrievals of aerosol effective radius (top frames; Figures 11a and 11b) and volume (bottom frames; Figures 11c and 11d) at 25.5 km based on the refractive indices in Table 1 and on the room temperature refractive indices measured by *Palmer and Williams* [1975] listed in Table 4. Retrievals of R_{eff} and V on the left,

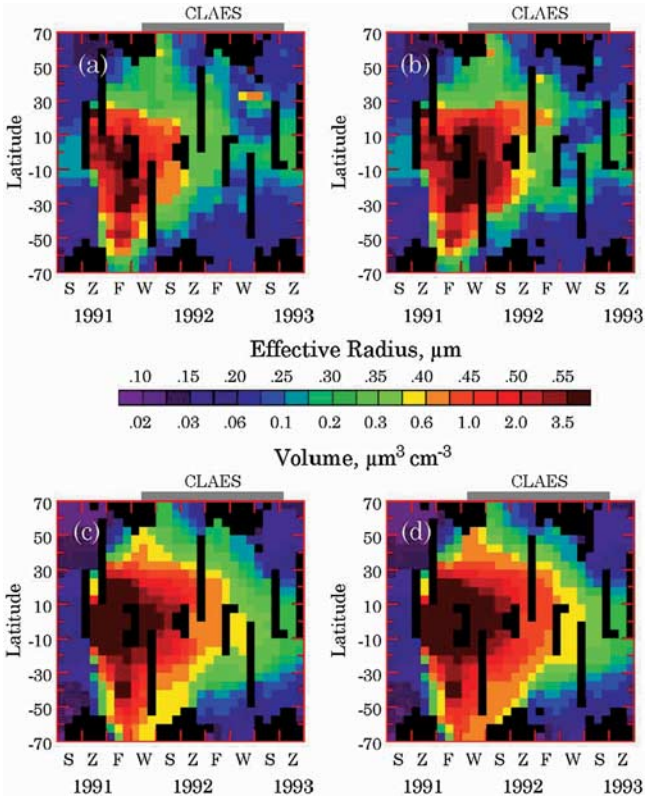

Figure 11. Sensitivity of LUT retrievals at 25.5 km to refractive index. Retrieved R_{eff} (Figures 11a and 11b), and volume (Figures 11c and 11d) based on values of refractive indices listed in Table 1 (left frames; Figures 11a and 11c) and in Table 4 (right frames; Figures 11b and 11d).

Figures 11a and 11c, are based on indices listed in Table 1, while retrievals on the right, Figures 11b and 11d, are based on the indices in Table 4. Palmer and Williams room temperature data are used for comparison because those indices have been the most widely used [e.g., *Arnold*, 1992; *Kiehl and Briegleb*, 1993; *Wooldridge et al.*, 1995] in modeling the optical properties of sulfuric acid aerosols.

[47] The largest noticeable discrepancy in retrieved values of R_{eff} occurs in the first half of 1992 in the tropics. For example, from January to June 1992 between 30°S and 30°N, the values of R_{eff} based on the set of indices in Table 4 (Figure 11b) are on average 7.5% larger than those values of R_{eff} based on the first set (Figure 11a). During this period, the LUT uses a composite of the CLAES 12.82 μm measurements with SAGE II data. (The period in which CLAES data were available is indicated by the gray bar at the top of each frame.) At times when only SAGE II data are available, no noticeable difference occurs between retrievals based on the two sets on indices (e.g., between Figures 11a and 11b or between Figures 11c and 11d). This suggests that the largest uncertainty in LUT retrievals due to the assumed optical constants arises from the value of refractive index at 12.82 μm.

[48] *Grainger et al.* [1995] show that the 12.82 μm absorption cross section per unit volume is constant when the size parameter $x = 2\pi r/\lambda$ is less than about 0.25. For wavelength $\lambda = 12.82$ μm, this corresponds to particle radii less than about 0.5 μm. Figure 11 shows that typical values of R_{eff} at this time and location are approximately 0.5 μm or less. Thus, for particles less than this limit the absorption at 12.82 μm is only weakly dependent on the shape of the distribution and can be approximated as a linear function of the aerosol volume. In this situation, measurements of absorption can be used to directly estimate aerosol volume. Furthermore, the absorption measurements at 12.82 μm approach the Rayleigh limit, and are proportional to the product of the imaginary refractive index and the aerosol mass [*Bohren and Huffman*, 1983]. Therefore an underestimate of the imaginary refractive index at 12.82 μm will result in an overestimate of aerosol mass. The imaginary index at 12.82 μm is smaller in the second set of indices (i.e., the room temperature estimates from *Palmer and Williams* [1975]) than in the first set (Tables 1 and 4). The second set of indices in Table 4 ascribes less absorptivity to the H_2SO_4 solution and therefore requires more aerosol mass to achieve the same absorption as a calculation based on the first set in Table 1. Thus retrievals of aerosol volume based on room temperature refractive indices from *Palmer and Williams* [1975] (Figure 11d) should be larger than those based on the *Tisdale et al.* [1998] indices (Figure 11c), which is the case.

10. Sensitivity to CLAES Measurement Wavelength

[49] Although the CLAES instrument measures profiles of aerosol absorption coefficient at eight wavelengths, the SAGE II/CLAES composite spectra used by the LUT algorithm only include CLAES measurements at 12.82 μm. The reason for selecting this wavelength is based on the fact that CLAES is an emission instrument. Thus the CLAES retrieval algorithm assumes that the measured intensity comes only from the emitting particles (i.e., scattering intensity is negligible). The intensity due to scattering can be minimized by choosing a wavelength where the absorption to scattering ratio is large. This occurs where the ratio of the imaginary-to-real refractive index is large. This is the case for the 7.96 μm and 12.82 μm channels of CLAES.

[50] The top frames in Figure 12 show the CLAES 7.96 μm (top left) and 12.82 μm (top right) extinction measurements at 25.5 km from January 1992 to May 1993. The bottom frames show corresponding retrievals of R_{eff} based on the CLAES measurements shown in the top frames. On average, values of R_{eff} based on the 7.96 μm extinction measurements are 12% larger than those based on 12.82 μm. The largest discrepancy between the two retrievals of R_{eff} occurs in early to mid-1992. During this period values of R_{eff} based on

Table 4. Complex Refractive Index at the SAGE II and CLAES Wavelengths From *Palmer and Williams* [1975] at 300 K and Interpolated to 70.85% H_2SO_4, Assuming the Environment Contains 3 ppmv of Water[a]

λ, μm	n	k	Source
0.385	1.4421	*	*Palmer and Williams* [1975]
0.453	1.4270	*	*Palmer and Williams* [1975]
0.525	1.4258	*	*Palmer and Williams* [1975]
1.020	1.4157	*	*Palmer and Williams* [1975]
12.82	1.6938	0.1663	*Palmer and Williams* [1975]

[a]The imaginary indices (k) marked * are $\leq 10^{-6}$.

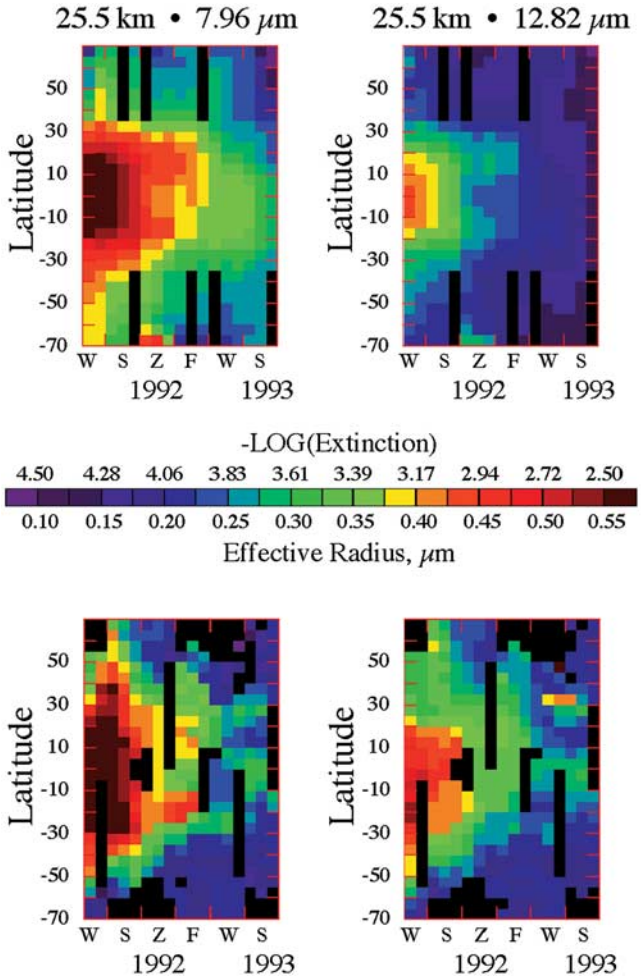

Figure 12. Sensitivity of LUT retrievals to CLAES measurement wavelength. Top frames: CLAES extinction at 7.96 μm (left) and 12.82 μm (right); Bottom frames: Retrievals of R_{eff} based on CLAES 7.96 μm measurements (left) and 12.82 measurements (right).

12.82 μm are consistent with estimates of R_{eff} of *Lambert et al.* [1997] at 25 km.

[51] Measurements at 12.82 μm are further from the strong H_2SO_4 absorption feature at 8.4 μm. Thus they are thus less subject to saturation in the tropics immediately following the Pinatubo eruption than are the 7.96 μm extinction measurements. In addition, the average percent precision is greater at 12.82 μm [*Massie et al.*, 1996] and there are numerous correlative studies using the CLAES 12.82 μm measurements. For these reasons, results presented in paper 2 are based solely on a compilation of SAGE II data with the CLAES 12.82 μm measurements.

11. Broader Applicability of the LUT Algorithm

[52] The use of the LUT algorithm is not restricted to the SAGE II or CLAES instruments, or to the wavelengths used by these instruments. It can be used with other remote sensing systems such as HALOE, POAM II and SAGE III. The number and range of wavelengths used by the algorithm can be extended to accommodate these instruments, provided reasonably accurate information about the refractive index is available at a given wavelength (see section 9 for guidance on required accuracy). The LUT technique can also retrieve aerosol properties from a set of hypothetical measurements at different wavelengths. Comparing retrieval errors for different sets of measurement wavelengths could potentially contribute to an instrument design with optimum wavelength channels in future remote sensing measurement missions.

12. Summary and Conclusions

[53] We have described the methods used to produce a global climatology of the stratospheric aerosol using data from two satellite instruments: the Stratospheric Aerosol and Gas Experiment (SAGE II) and the Cryogenic Limb Array Etalon Spectrometer (CLAES). The climatology includes values and uncertainties of measured extinction and optical depth, and of retrieved particle effective radius R_{eff}, distribution width σ_g, surface area S and volume V. As a basis for aerosol retrievals, a multiwavelength look-up table (LUT) algorithm was developed. The algorithm matches satellite-measured extinction ratios to precomputed ratios that are based on a range of unimodal lognormal size distributions. It can retrieve information about distribution width by noting the range of σ_g values for which computed extinction spectra are consistent with satellite measurements. For cases where the basic algorithm does not find an acceptable match between measured and precomputed extinction spectra, the LUT is augmented with a parameter search technique (PST). The combination of the LUT and PST with data from both satellites allows us to retrieve values of R_{eff}, σ_g, S, and V over a wider range of conditions and from a wider range of wavelengths than used by other methods. The greater wavelength range helps constrain retrieved results, especially in postvolcanic conditions when particle sizes are greatly increased and SAGE II extinction spectra become essentially independent of wavelength.

[54] Our method includes an altitude- and time-dependent procedure that uses bimodal size distributions from in situ measurements to estimate the bias and uncertainty introduced by assuming a unimodal functional form. Correcting for this bias reduces uncertainty in retrievals of R_{eff}, S and V by about 7%, 5% and 1% (averaged over all altitude bands), leaving remaining uncertainties from the unimodal assumption of about ±18%, ±20% and ±20%, respectively. Additional uncertainties, which result from measurement error and spatiotemporal variability, are evaluated by propagating input uncertainties through the LUT-PST algorithm. Resulting overall uncertainties in retrieved R_{eff}, S and V vary with location and aerosol condition (e.g., volcanic versus nonvolcanic) and are reported in paper 2 along with the climatology of R_{eff}, S and V. In this paper we examine the sensitivity of our retrievals to refractive index and measurement wavelength. We find, for example, that changing refractive index from a value for the stratospheric temperature of 215 K to that for 300 K can increase retrieved R_{eff} by ~7.5%, owing largely to effects at the CLAES 12.82 μm wavelength. When only SAGE II wavelengths are used, corresponding changes in R_{eff} are much smaller.

[55] The LUT algorithm can be applied to other wavelengths and data from other instruments, such as HALOE, POAM II and SAGE III. In the accompanying paper [*Bau-*

man et al., 2003] it is used with SAGE II and CLAES data to derive a stratospheric aerosol climatology extending over the 14-year, 9-month period December 1984 to August 1999.

[56] **Acknowledgments.** This research was supported by NASA's Atmospheric Chemistry Modeling and Analysis Program through a SAGE II Science Team grant. The Cryogenic Limb Array Etalon Spectrometer (CLAES) absorption data were produced and distributed by the Upper Atmosphere Research Satellite (UARS) Project and the Distributed Active Archive Center at the Goddard Space Flight Center, Greenbelt, Maryland, respectively. These activities were sponsored by NASA's Mission to Planet Earth Program. The Stratospheric Aerosol and Gas Experiment II (SAGE II) extinction data were developed by NASA Langley Research Center and processed at the NASA LaRC Aerosol Research Branch. We appreciate unpublished data sets supplied to us by Terry Deshler. John Livingston's guidance and assistance are greatly appreciated as is technical support by Stephanie Ramirez.

References

Arnold, F., Stratospheric aerosol increases and ozone destruction: Implications for mass spectrometer measurements, *Ber. Bunsenges. Phys. Chem.*, *96*, 339–350, 1992.

Bauman, J. J., Stratospheric aerosol climatology derived from satellite solar occultation and infrared emission measurements, Ph.D. dissertation, 237 pp., State Univ. of New York, Stony Brook, 2000.

Bauman, J. J., P. B. Russell, M. A. Geller, and P. Hamill, A stratospheric aerosol climatology from SAGE II and CLAES measurements: 2. Results and comparisons, 1984–1999, *J. Geophys. Res.*, *108*, doi:10.1029/2002JD002993, in press, 2003.

Ben-David, A., B. Herman, and J. Reagan, Inverse problem and the pseudoempirical orthogonal function method of solution: 1. Theory, *Appl. Opt.*, *27*, 1235–1242, 1988.

Bevington, P. R., *Data Reduction and Error Analysis for the Physical Sciences*, 336 pp., McGraw-Hill, New York, 1969.

Bevington, P. R., and D. K. Robinson, *Data Reduction and Error Analysis for the Physical Sciences*, 2nd ed., p. 198, McGraw-Hill, New York, 1992.

Bohren, C., and D. Huffman, *Absorption and Scattering of Light by Small Particles*, John Wiley, New York, 1983.

Brasseur, G., C. Granier, and S. Walters, Future changes in stratospheric ozone and the role of heterogeneous chemistry, *Nature*, *348*, 626–628, 1990.

Dennis, R., *Handbook on Aerosols*, Energy Res. and Dev. Admin., Bedford, Mass., 1976.

Deshler, T., and S. J. Oltmans, Vertical profiles of volcanic aerosol and polar-stratospheric clouds above Kiruna, Sweden: Winters 1993 and 1995, *J. Atmos. Chem*, *30*, 11–23, 1998.

Deshler, T., D. J. Hofmann, B. J. Johnson, and W. R. Rozier, Balloonborne measurements of the Pinatubo aerosol size distribution and volatility at Laramie, Wyoming during the summer of 1991, *Geophys. Res. Lett.*, *19*, 199–202, 1992.

Deshler, T., B. J. Johnson, and W. R. Rozier, Balloonborne measurements of Pinatubo aerosol during 1991 and 1992 at 41 N: Vertical profiles, size distribution, and volatility, *Geophys. Res. Lett.*, *20*, 1435–1438, 1993.

Dutton, E. G., and J. R. Christy, Solar radiative forcing at selected locations and evidence for global lower tropospheric cooling following the eruptions of El Chichón and Pinatubo, *Geophys. Res. Lett.*, *19*, 2313–2316, 1992.

Goodman, J., K. G. Snetsinger, R. F. Pueschel, G. V. Ferry, and S. Verma, Evolution of Pinatubo aerosol near 19-km altitude over western North America, *Geophys. Res. Lett.*, *21*, 1129–1132, 1994.

Grainger, R. G., A. Lambert, C. D. Rodgers, F. W. Taylor, and T. Deshler, Stratospheric aerosol effective radius, surface area and volume estimated from infrared measurements, *J. Geophys. Res.*, *100*, 16,507–16,518, 1995.

Hansen, J., and L. Travis, Light scattering in planetary atmospheres, *Space Sci. Rev.*, *16*, 527–610, 1974.

Hansen, J. E., W. Rossow, and I. Fung, The missing data on global climate change, *Issues Sci. Technol.*, *7*, 62–69, 1990.

Hofmann, D. J., and J. M. Rosen, Stratospheric sulphuric acid mass fraction and mass estimate for the 1982 volcanic eruption of El Chichón, *Geophys. Res. Lett.*, *10*, 313–316, 1983.

Hofmann, D. J., and S. Solomon, Ozone destruction through heterogeneous chemisty following the eruption of El Chichón, *J. Geophys. Res.*, *94*, 5029–5041, 1989.

Jensen, E. J., and O. B. Toon, The potential effects of volcanic aerosols on cirrus cloud microphysics, *Geophys. Res. Lett.*, *19*, 1759–1762, 1992.

Kent, G. S., P.-H. Wang, M. P. McCormick, and K. M. Skeens, Multiyear measurements of upper tropospheric aerosol characteristics, *J. Geophys. Res.*, *100*, 13,875–13,900, 1995.

Kiehl, J. T., and B. P. Briegleb, The relative roles of sulfate aerosols and greenhouse gases in climate forcing, *Science*, *260*, 311–314, 1993.

Kinne, S., O. B. Toon, and M. J. Prather, Buffering of stratospheric circulation by changing amounts of tropical ozone: A Pinatubo case study, *Geophys. Res. Lett.*, *19*, 1927–1930, 1992.

Knollenberg, R. G., and D. Huffman, Measurements of the aerosol size distributions in the El Chichón cloud, *Geophys. Res. Lett.*, *10*, 1025–1028, 1983.

Lacis, A. A., J. E. Hansen, and M. Sato, Climate forcing by stratospheric aerosols, *Geophys. Res. Lett.*, *19*, 1607–1610, 1992.

Lambert, A., R. G. Grainger, C. D. Rodgers, F. W. Taylor, J. L. Mergenthaler, J. B. Kumer, and S. T. Massie, Global evolution of the Mt. Pinatubo volcanic aerosols observed by the infrared limb-sounding instruments CLAES and ISAMS on the Upper Atmosphere Research Satellite, *J. Geophys. Res.*, *102*, 1495–1512, 1997.

Lenoble, J., and C. Brogniez, A comparative review of radiation aerosol models, *Beitr. Phys. Atmos.*, *57*, 1–20, 1984.

Liu, Y., W. P. Arnott, and J. Hallett, Particle size distribution retrieval from multispectral optical depth: Influences of particle nonsphericity and refractive index, *J. Geophys. Res.*, *104*, 31,753–31,762, 1999.

Livingston, J. M., Data analysis and presentation in support of SAGE II Science Team inves-tigations, *Q. Progress Rep. 10*, contract NAS2-13989, SRI Int., Menlo Park, Calif., July 1996.

Massie, S. T., et al., Validation studies using multiwavelength Cryogenic Limb Array Etalon Spectrometer (CLAES) observations of stratospheric aerosol, *J. Geophys. Res.*, *101*, 9757–9774, 1996.

McCormick, M. P., L. W. Thomason, and C. R. Trepte, Atmospheric effects of the Mt. Pinatubo eruption, *Nature*, *373*, 399–404, 1995.

Minnis, P., E. F. Harrison, L. L. Stowe, G. G. Gibson, P. M. Denn, D. R. Doelling, and W. L. Smith Jr., Radiative climate forcing by Mount Pinatubo eruption, *Science*, *259*, 1411–1415, 1993.

Oberbeck, V. R., E. F. Danielsen, K. G. Snetsinger, G. V. Ferry, W. Fong, and D. M. Hayes, Effect of the eruption of El Chichon on stratospheric aerosol size and composition, *Geophys. Res. Lett.*, *10*, 1021–1024, 1983.

Palmer, K. F., and D. Williams, Optical constants of sulfuric acid: Application to the clouds of Venus?, *Appl. Opt.*, *14*, 208–219, 1975.

Prather, M., Catastrophic loss of stratospheric ozone in dense volcanic clouds, *J. Geophys. Res.*, *97*, 10,187–10,191, 1992.

Pueschel, R. F., et al., Condensed nitrate, sulfate, and chloride in Antarctic stratospheric aerosols, *J. Geophys. Res.*, *94*, 11,271–11,284, 1989.

Pueschel, R. F., K. G. Snetsinger, P. B. Russell, S. A. Kinne, and J. M. Livingston, The effects of the 1991 Pinatubo volcanic eruption on the optical and physical properties of stratospheric aerosols, in *Proceedings of IRS92: Current Problems in Atmospheric Radiation*, edited by S. Keevalik, pp. 183–186, A. Deepak, Hampton, Va., 1992.

Pueschel, R. F., J. M. Livingston, P. B. Russell, and S. Verma, Physical and optical properties of the Pinatubo volcanic aerosol: Aircraft observations with impactors and a suntracking photometer, *J. Geophys. Res.*, *95*, 12,915–12,922, 1994.

Rampino, M. R., and S. Self, Sulphur-rich volcanic eruptions and stratospheric aerosols, *Nature*, *310*, 677–679, 1984.

Robock, A., Volcanic effects on climate, in *Volcanism-Climate Interactions*, edited by L. S. Walter and S. de Silva, *NASA Conf. Publ., CP-10,062*, E1–E16, 1991.

Russell, P. B., et al., Post-Pinatubo optical depth spectra vs. latitude and vortex structure: Airborne tracking sunphotometer measurements in AASE II, *Geophys. Res. Lett.*, *20*, 2571–2574, 1993a.

Russell, P. B., et al., Pinatubo and pre-Pinatubo optical depth spectra: Mauna Loa measurements, comparisons, inferred particle size distributions, radiative effects, and relationship to lidar data, *J. Geophys. Res.*, *98*, 22,969–22,985, 1993b.

Russell, P. B., et al., Global to microscale evolution of the Pinatubo volcanic aerosol derived from diverse measurements and analyses, *J. Geophys. Res.*, *101*, 18,745–18,764, 1996.

Steele, H. M., and P. Hamill, Effects of temperature and humidity on the growth and optical properties of sulphuric acid water droplets in the stratosphere, *J. Aerosol Sci.*, *12*, 517–528, 1981.

Thomason, L. W., A diagnostic stratospheric aerosol size distribution inferred from SAGE II measurements, *J. Geophys. Res.*, *96*, 22,501–22,508, 1991.

Thomason, L. W., and L. R. Poole, Use of stratospheric aerosols properties as diagnostics of Antarctic vortex processes, *J. Geophys. Res.*, *98*, 23,002–23,012, 1993.

Tisdale, R. T., D. L. Glandorf, and M. A. Tolbert, Infrared optical constants of low-temperature H_2SO_4 solutions representative of stratospheric sulfate aerosols, *J. Geophys. Res.*, *103*, 25,353–25,370, 1998.

Wang, P.-H., M. P. McCormick, T. J. Swissler, M. T. Osborn, W. H. Fuller, and G. K. Yue, Inference of stratospheric aerosols composition and size distribution from SAGE II satellite measurements, *J. Geophys. Res.*, *94*, 8435–8446, 1989.

Wooldridge, P. J., R. Zhang, and M. J. Molina, Phase equilibria of H_2SO_4, HNO_3, HCl hydrates and thee composition of polar stratospheric clouds, *J. Geophys. Res.*, *100*, 1389–1396, 1995.

Young, R., H. Houben, and O. Toon, Radiatively forced dispersion of the Mt. Pinatubo volcanic cloud and induced temperature perturbations in the stratosphere during the first few months following the eruption, *Geophys. Res. Lett.*, *21*, 369–372, 1994.

Yue, G. K., and A. Deepak, Retrievals of stratospheric aerosols size distribution from atmosphere extinction of solar radiation at two wavelengths, *Appl. Opt.*, *22*, 1639–1645, 1983.

Yue, G. K., and A. Deepak, Latitudinal and altitudinal variation of size distribution of stratospheric aerosols inferred from SAGE aerosol extinction coefficient measurements at two wavelengths, *Geophys. Res. Lett.*, *11*, 999–1002, 1984.

Yue, G. K., L. R. Poole, P.-H. Wang, and E. W. Chiou, Stratospheric aerosol acidity, density, and refractive index deduced from SAGE II and NMC temperature data, *J. Geophys. Res.*, *99*, 3727–3738, 1994.

J. J. Bauman and P. B. Russell, Advanced Projects Branch, NASA Ames Research Center, Mail Stop 244-14, Moffett Field, CA 94035-1000, USA. (jbauman@mail.arc.nasa.gov; prussell@mail.arc.nasa.gov)

M. A. Geller, Institute for Terrestrial and Planetary Atmospheres, State University of New York at Stony Brook, Stony Brook, NY 11794-5000, USA. (marvin.geller@sunysb.edu)

P. Hamill, Department of Physics, San Jose State University, 1 Washington Square, San Jose, CA 95192, USA. (hamill@stratus.arc.nasa.gov)